# Analysis of the Quality Control Measurements performed on the Absorbers produced for the Module 0 of the ATLAS Electromagnetic EndCap Calorimeter

L. Labarga, P. Romero
*University Autonoma Madrid*

**Internal number for this document: ABS.QAP.00.QRa.1**

11/01/1999

**Abstract**

This note deals with the absorbers produced for the Module 0 of the ATLAS Electromagnetic End Cap Calorimeter (M00). After giving a brief overview of the production process, we describe the quality control procedure. The bulk of the note is dedicate to the analysis of the different geometrical measurements performed on the absorbers and the discussion of the results.

# 1 Introduction.

## 1.1 Overview of the absorber production for EMEC-M00.

The absorber production for M00 can be naturally divided in the 10 cycles corresponding to the 10 autoclave pressure-temperature cycles which were necessary for that production.

Typically, the autoclave was filled with 10 large moulds (for curing 10 outer absorbers) and 4 small moulds (for curing 4 inner absorbers). We will call them 10+4 cycles. Exceptions occurred in the cycles no.:

- **$8^{th}$:** one small mould less (i.e. it was a 10+3 cycle), since the corresponding small absorber was destroyed during the bending process due to a press failure.

- **$9^{th}$, $10^{th}$:** only 2 and 1 small moulds (i.e. 10+2 and 10+1 cycles respectively) due to lack of some materials.

The total number of pieces produced for M00 was therefore 100 outer and 34 inner absorbers.

The yield was almost 100%. As mentioned above only one absorber was destroyed during the production process. However, one may contemplate a reduction of this yield based on quality considerations. This will be discussed extensively in sections 4 and 5 but we can anticipate that only 2 outer and 2 inner absorbers showed worse quality than the rest (being the reasons for that known).

The dates for the 10 M00 cycles are shown in Fig. 1. The lead was cleaned two days before processing. Just after cleaned, the lead was stored inside a sealed box with an anti-humidity product inside. The sealed box was only open at the very moment of the processing.

PLAN FABRICACION M0 (*versión 27/03/98*)

| | | Fibertecnic | | | Mendiaraiz | | | Aratz | |
|---|---|---|---|---|---|---|---|---|---|
| Ciclo no. | Sem. no. | No. absorbers | Moldeado | Autoclave y desmoldeado | Limpieza plomo | No. planchas a limpiar | Plomo en FIBER | No. barras a proveer | Barras en FIBER |
| 1 | 14 | 10G+4P | 01/04 | 03/04 | 30/03 | 10G+4P | 31/03 | 2x(10G+4P) | 31/03 |
| 2 | 19 | 10G+4P | 06/05 | 07/05 | 04/05 | 10G+4P | 05/05 | 2x(10G+4P) | 05/05 |
| 3 | 21 | 10G+4P | 20/05 | 21/05 | 18/05 | 10G+4P | 19/05 | 2x(10G+4P) | 19/05 |
| 4 | 22 | 10G+4P | 27/05 | 28/05 | 25/05 | 10G+4P | 26/05 | 2x(10G+4P) | 26/05 |
| 5 | 23 | 10G+4P | 03/06 | 04/06 | 01/06 | 10G+4P | 02/06 | 2x(10G+4P) | 02/06 |
| 6 | 24 | 10G+4P | 10/06 | 11/06 | 08/06 | 10G+4P | 09/06 | 2x(10G+4P) | 09/06 |
| 7 | 25 | 10G+4P | 17/06 | 18/06 | 15/06 | 10G+4P | 16/06 | 2x(10G+4P) | 16/06 |
| 8 | 26 | 10G+4P | 24/06 | 25/06 | 22/06 | 10G+4P | 23/06 | 2x(10G+4P) | 23/06 |
| 9 | 27 | 10G+4P | 30/06 | 01/07 | 26/06 | 10G+4P | 29/06 | 2x(10G+4P) | 29/06 |
| 10 | 28 | 10G+4P | 08/07 | 09/07 | 06/07 | 10G+4P | 07/07 | 2x(10G+4P) | 07/07 |

Figure 1: The dates for the 10 cycles of the M00 production (in Spanish). On top are the companies where the different activities were carried out. *Moldeado:* flat sandwich forming and bending. *Limpieza plomo:* the lead cleaning. *Barras:* longitudinal bars.

## 1.2 A typical 10+4 cycle.

The dates for the activities within a typical 10+4 cycle were as follows:

- *Wednesday:* The prepreg sheets are cut and the longitudinal bars cleaned. A few absorbers are stacked, bent and put in place on the moulds.

- *Thursday:* The rest of the absorbers are stacked, bent and put in place on the corresponding moulds. The moulds are closed with the vacuum bags.

- *Friday:* Autoclave cycle.

- *Monday:* Take the cured absorbers out of the moulds. Start cleaning the absorbers from rests of resin.

- *Tuesday:* End cleaning of absorbers. If there is time start cuting the prepreg sheets for the next cycle.

- *next Wednesday:*

    1. Quality control (by quality control Dept).

2. Start new cycle (by absorber crew).

- *next Thursday:*

1. Packing and shipping (by warehouse people). END of the cycle.
2. End bending next cycle (by absorber crew).

The above rate of 1 cycle per week can certainly be increased for the full production. The goal is 1.2 cycles a week.

## 1.3 Absorber naming in this note

Along this note we will be naming the absorbers with the following convention suited for production tracing:

**XIII_JJ_mKKcLL**

where

"X" can be either "b" for the outer absorbers (from b-ig) or "s" for the inner absorber (from s-mall),

"III" is the number of the lead plate forming the absorber (the lead plates are numbered in the UAM at the time of the ultrasound thickness measurement, this number is marked mechanically on a corner of the plate),

"JJ" is the number of the mould in which the absorber has been cured; it ranges from 1 to 10 (1 to 4) for the outer (inner) absorbers,

"KK" is the EMEC module number (for obvious reasons in this note will be always 00),

"LL" is the number of the cycle in which the absorber has been produced.

For example b076_10_m00c02 is the outer absorber made in mould no. 10 in the $2^{nd}$ cycle of M00 and it has inside the lead plate no. 76. s031_01_m00c01 is the inner absorber made in mould no. 1 in the $1^{st}$ cycle of M00 and it has inside the lead piece no. 31.

In some cases and due to several reasons that we will try to solve for the production, the no. in the lead plate was missing and therefore it was impossible to link the absorber with its corresponding lead plate. In those cases, the "III" is replaced by an "unMM" where "MM" counts the number of incidences of this type.

When scatter plotting results from several absorbers, we will assign the same type of marker to results from absorbers made in the same mould. Different marker types will be used for the different moulds. The marker type assignment versus number of mould is shown in Fig. 2. There will be a few exceptions to this rule for which the marker assignment will be hopefully obvious.

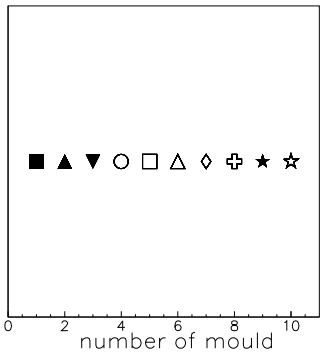


Figure 2: Types of markers used when plotting results from absorbers made at different moulds.

# 2 Quality Control Procedure.

Two types of quality control procedures were carried out; extensive, in 10% of the produced absorbers, and basic in the rest of them. As an exception and in order to check that the whole system worked correctly, the extensive control was carried out also for all the absorbers produced in the first 10+4 cycle.

The 10% of the absorbers for which the extensive quality control was applied were chosen such that one absorber from every mould was measured along the 10 cycles of a module. The idea behind is to be able to study possible long term effects in the moulds.

## 2.1 Extensive Quality Control.

It consists of:

1. Optical inspection looking for defects at the surface, unglued areas, holes between the lead and stainless steel at the folds etc. Also the straightness of the longitudinal bars was carefully checked for the last half of the cycles.

2. Thickness measurement of all surfaces between folds at the obtuse and acute angled sides of the absorber. More details will be given in section 3.

3. Measurement of the absorber length at two fixed transverse sections (with a precision meter). Fig. 3 show the geometrical location of these measurements in both outer and inner absorbers.

4. 3-D mapping with a 3-D measurement machine. This will be explained in detail in section 3.2.

5. Measurement of the absorber width at the longitudinal bar ends also with the 3-D measurement machine. Fig. 3 show the geometrical location of these measurements in both outer and inner absorbers.

With the results of the different measurements a quality control sheet was filled. An example of sheet filled can be seen in Fig. 4-top for outer and inner absorbers.

## 2.2 Basic Quality Control.

It consists of:

1. Optical inspection looking for defects at the surface, unglued areas, holes between the lead and stainless steal at the folds etc. Also the straightness of the longitudinal bars was carefully checked for the last half of the cycles. This item is exactly that of the extensive quality control.

2. Thickness measurement of 4 (3) surfaces between folds at the obtuse and acute angled sides of the outer (inner) absorber respectively. The surfaces measured were always the same and their locations are shown in Fig. 3 for both inner and outer absorbers.

3. Measurement of the absorber width at the longitudinal bar ends (with a big caliber) and the absorber length at two fixed transverse sections (with a regular meter). Fig. 3 show the geometrical location of these measurements in both outer and inner absorbers.

With the results of the different measurements a quality control sheet was filled. An example of sheet filled can be seen in Fig. 4-bottom for outer and inner absorbers.

## 2.3 Tolerances Considered.

In order to have a reference for the goodness of the measurement results, we have established tolerances for the different variables under study as follows.

They are based on the Liquid Argon gap uniformity necessary to achieve a local signal uniformity of 1% R.M.S.. This requirement is the same from which the specifications for the lead thickness uniformity were derived.

The relationship between the Liquid Argon gap ($g$) and signal ($S$) uniformities is (see for example [1]):

$$\frac{\Delta g}{g} = \frac{1.}{0.3} \times \frac{\Delta S}{S}$$

were the factor 1/0.3 comes from the dependence of the drift velocity on the electric field (and therefore the high voltage).

Taking $\Delta S/S = 1\%$ we obtain a $\Delta g/g = 3.\hat{3}$ %. However, in order to give room for quadratic sums of independent effects we have lowered our target $\Delta g/g$ for independent variables to

$$\frac{\Delta g}{g} = 2\%$$

which is approximately $3.\hat{3}/\sqrt{3}$. I.e. three independent effects, each introducing non-uniformities within our target tolerance will produce, when summed in quadrature, a global non-uniformity in the signal of the order of that induced by the non-uniformities in the lead thickness.

The above requirement translate into tolerances for thicknesses, angles and spatial coordinates as derived in [2].

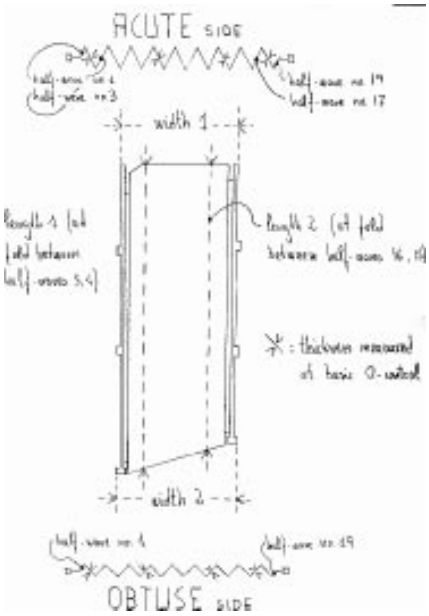


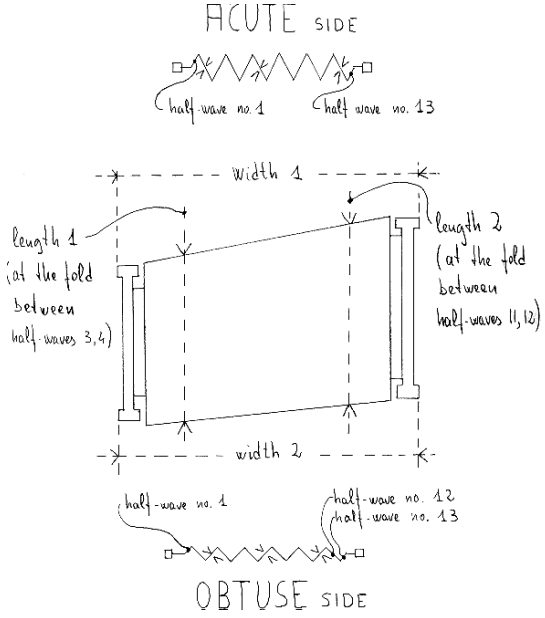


Figure 3: Sketches of outer (top) and inner (bottom) absorbers showing the location of the width, length and thickness measurement in a basic quality control. Also the numbering of the half-wave surfaces is shown.

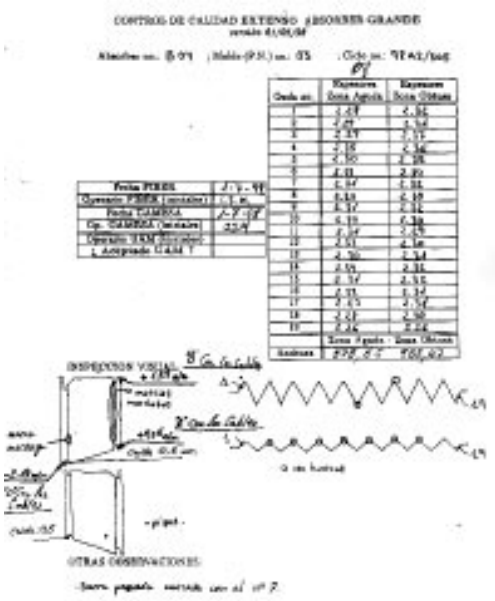

CONTROL DE CALIDAD EXTENSO ABSORBER PEQUEÑO
versión 21/05/98

Absorber no.: 526 ; Molde (P.N.) no.: 01 ; Ciclo no.: 9841/377

| Onda no. | Espesores Zona Aguda | Espesores Zona Obtusa |
|---|---|---|
| 1 | 2.77 | 2.77 |
| 2 | 2.76 | 2.90 |
| 3 | 2.82 | 2.86 |
| 4 | 2.85 | 2.90 |
| 5 | 2.82 | 2.90 |
| 6 | 2.83 | 2.91 |
| 7 | 2.85 | 2.88 |
| 8 | 2.86 | 2.81 |
| 9 | 2.85 | 2.84 |
| 10 | 2.86 | 2.89 |
| 11 | 2.90 | 2.83 |
| 12 | 2.84 | 2.84 |
| 13 | 2.83 | 2.78 |
| | Zona Aguda | Zona Obtusa |
| Anchura | 586,05 | 586,71 |

| | |
|---|---|
| Fecha FIBER | 24-6-98 |
| Operario FIBER (iniciales) | I.S.M. |
| Fecha GAMESA | 25-6-98 |
| Op. GAMESA (iniciales) | I.T.M. |
| Operario UAM (iniciales) | |
| ¿ Aceptado UAM ? | |

INSPECCION VISUAL:

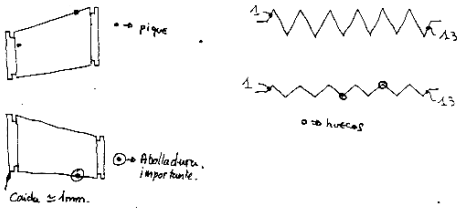


OTRAS OBSERVACIONES:

CONTROL DE CALIDAD BASICO ABSORBER GRANDE
versión 21/05/98

Absorber no.: 827 ; Molde (P.N.) no.: 03 ; Ciclo no.: 9841/412

| | |
|---|---|
| Fecha | 9-9-98 |
| Operario (iniciales) | I.S.M. |

CONTROL GEOMETRICO:

| Concepto | Rango | Resultado | ¿ Pasa ? |
|---|---|---|---|
| Espesor 1 (Zona Aguda) | 2.27 - 2.35 | 2'31 | |
| Espesor 2 (Zona Aguda) | 2.30 - 2.38 | 2'34 | |
| Espesor 3 (Zona Aguda) | 2.29 - 2.38 | 2'34 | |
| Espesor 4 (Zona Aguda) | 2.24 - 2.34 | 2'29 | |
| Espesor 5 (Zona Obtusa) | 2.34 - 2.42 | 2'34 | |
| Espesor 6 (Zona Obtusa) | 2.31 - 2.40 | 2'33 | |
| Espesor 7 (Zona Obtusa) | 2.29 - 2.38 | 2'33 | |
| Espesor 8 (Zona Obtusa) | 2.28 - 2.37 | 2'33 | |
| Anchura 1 (Zona Aguda) | 578.1 - 578.9 | 578'6 | |
| Anchura 2 (Zona Obtusa) | 586.7 - 587.9 | 586'9 | |
| Longitud 1 | 1410.5 - 1411.5 | 1411,3 | |
| Longitud 2 | 1354.0 - 1355.0 | 1354,9 | |
| ¿ Pasa Global ? si NO, ¿ Pasa UAM ? | | | |

INSPECCION VISUAL:

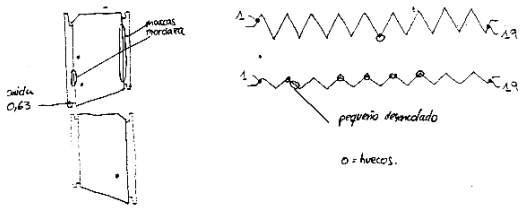


OBSERVACIONES:

CONTROL DE CALIDAD BASICO ABSORBER PEQUEÑO
versión 21/05/98

Absorber no.: 46 ; Molde (P.N.) no.: 01 ; Ciclo no.: 9842/316

| | |
|---|---|
| Fecha | 3-6-98 |
| Operario (iniciales) | I.S.M. |

CONTROL GEOMETRICO:

| Concepto | Rango | Resultado | ¿ Pasa ? |
|---|---|---|---|
| Espesor 1 (Zona Aguda) | 2.75 - 2.84 | 2.77 | |
| Espesor 2 (Zona Aguda) | 2.86 - 2.94 | 2.90 | |
| Espesor 3 (Zona Aguda) | 2.81 - 2.90 | 2.82 | |
| Espesor 4 (Zona Obtusa) | 2.81 - 2.90 | 2.86 | |
| Espesor 5 (Zona Obtusa) | 2.84 - 2.94 | 2.78 | |
| Espesor 6 (Zona Obtusa) | 2.81 - 2.89 | 2.85 | |
| Anchura 1 (Zona Aguda) | 585.7 - 586.7 | 586.1 | |
| Anchura 2 (Zona Obtusa) | 586.5 - 587.1 | 586.9 | |
| Longitud 1 | 317.3 - 318.3 | 317.3 | |
| Longitud 2 | 346.0 - 347.0 | 346.4 | |
| ¿ Pasa Global ? si NO, ¿ Pasa UAM ? | | | |

INSPECCION VISUAL:

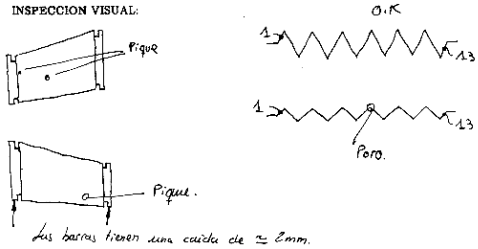


OBSERVACIONES:

Figure 4: Examples of quality control sheets filled with data from random absorbers. The top (bottom) sheets correspond to extensive (basic) quality control from outer (left) and inner (right) absorbers.

# 3 Methods of measurement

As mentioned in section 2 there are four different types of mechanical measurements in the quality control procedure, namely thicknesses, absorber width and length and 3-D mapping.

The absorber width and length are measured directly with a big caliber and a precision meter respectively as described in section 2.

## 3.1 Measurement of thicknesses.

Absorber thicknesses were measured only in the flat surfaces of the waves between the folds (notice that in reality those areas are flat only locally, since they are ruled surfaces whose angle is varying longitudinally). A regular Palmer micrometer was used. Due to the small area that regular Palmers can access, thicknesses were measured only at the edge of the absorbers in both obtuse and acute sides. The numbering for the surfaces measured are shown in Fig. 3 for both outer and inner absorbers.

## 3.2 3-D Mapping.

For the 3-D mapping, two especial jigs (one for each type of absorbers) were designed and fabricated. The idea behind the design was to place the absorbers for measurement in a situation close to that in the detector structure. Their manufacturing drawings can be found in [3]. Some details follow:

1. The jig positions the absorber flat, i.e. the absorber symmetry plane is parallel to the granite table of the measuring machine.
2. This positioning is made by means of pins which are finally inserted into the precision holes that the longitudinal bars have for positioning into the structure.
3. The pins are guided horizontal by means of pass-through holes precisely machined in the jig.
4. Transversally, the absorber is precisely positioned w.r.t. the jig only along the external[1] longitudinal bar. Once this longitudinal bar is positioned, it is firmly attached to the jig. The internal longitudinal bar remains transversely free in the jig. The idea behind is not to force transversally the absorber to any determined shape, in order to study and measure its transversal shrinkage (see secs. 4 and 5).
5. In order to minimize gravitational sagging when the absorber is in position in the jig, this has several transverse bars, precisely located, on which the absorber rests.

Fig. 5-top shows the measuring jig for the outer absorber positioned on the granite table. Fig. 5-bottom shows one outer absorber already positioned and fixed to the measuring jig.

In order to study the reproducibility properties of the absorbers, the reference frame for the measurements is determined by the jig and the granite table (i.e. it is independent of the absorber). See Fig. 6 for the location of the absorber in this reference frame.

The main measurement consist of a mapping in which the 3-D machine measures the Z coordinates of a predefined grid of X,Y points. Those X,Y points are arranged in the eight scan lines (seven for the inner absorbers) shown in Fig. 6. In each scan line 5 points are measured in each half-wave surface ( except for the most internal and external surfaces in which, given their small size only two points are measured). A straight line is fitted to every set of 5 points. With those lines, half-wave surface angles and fold's coordinates are determined as sketched in Fig. 6.

Also, for extensive quality controls, the absorber widths specified in Fig. 3 are measured with the 3-D machine.

Some problems in the outer absorber measuring jig have been identified during the analysis of the M00 measurements (see secs. 4 and 5):

1. The most acute side of the absorber is not perfectly fixed to the jig. The reason is known and it is a consequence of the fact than when the jig was designed, we did not take into account that the positioning hole of the longitudinal bar at that side was going to be filled with the inserts for attaching to the detector structure. The temporary fix that we made to overcome the problem was clearly insufficient, and effectively, the absorber remained free at that side during the measurement.

[1] Along this note the "internal" and "external" parts of the absorber refer to those facing the ATLAS IP and the hadronic EndCap respectively, once the component is inside the ATLAS detector.

2. The jig was also not properly fixing the absorber height at its most obtuse internal side. The reason being in this case that the clearance left for the pass-trough holes of the positioning pins (the same for all of them) was too large w.r.t. the small diameter of that particular pin and therefore the pass-trough hole was not defining the direction of this pin sufficiently.

We will try to fix those problems for the production.

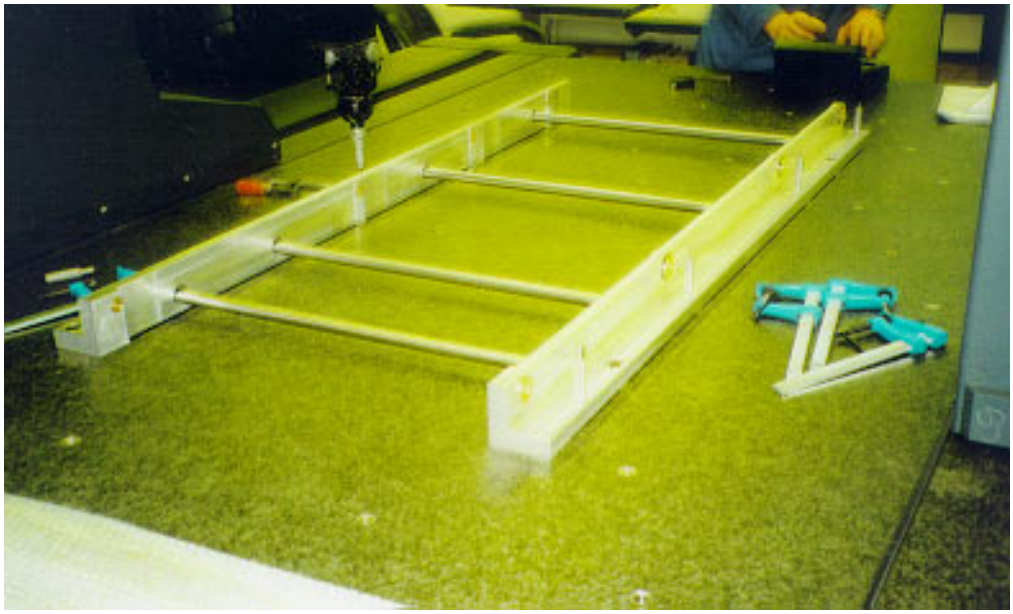

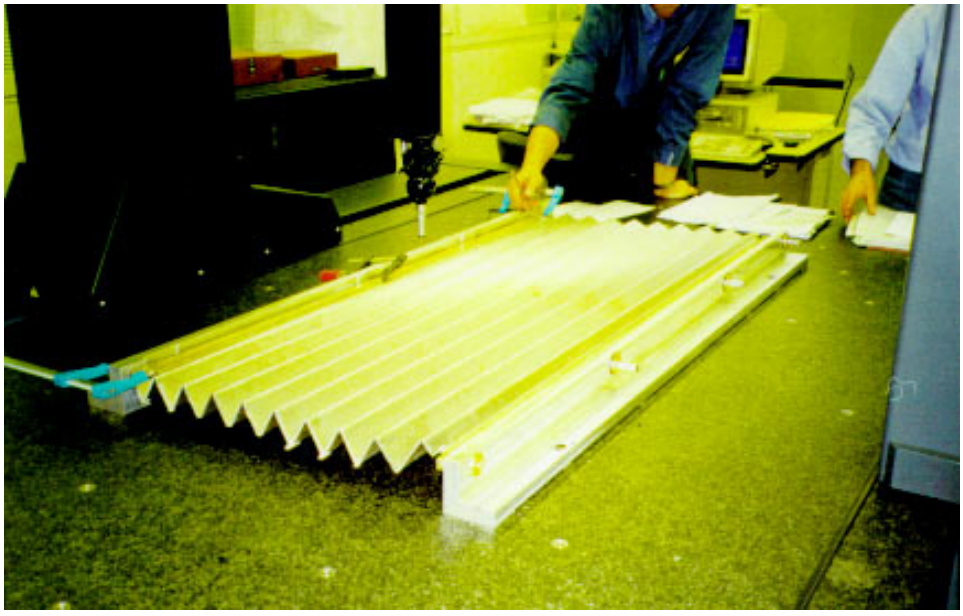

Figure 5: Photographs of the outer absorber 3-D measuring jig.

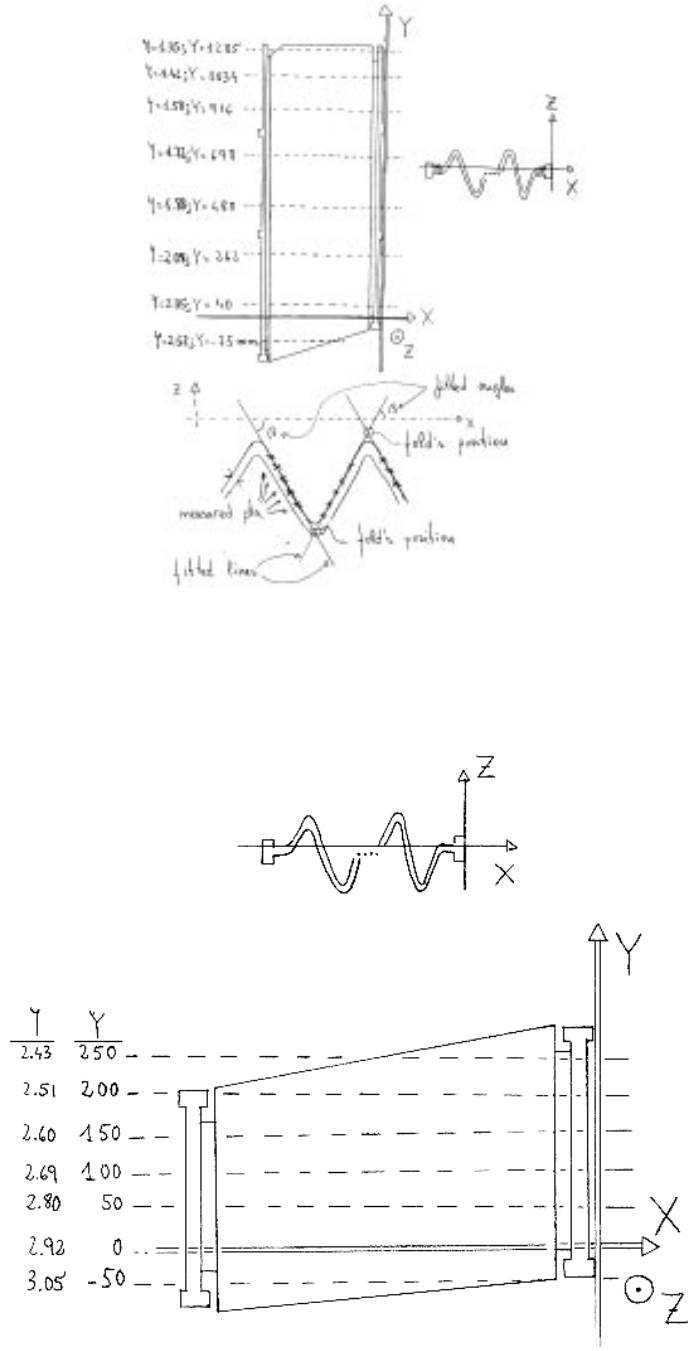


Figure 6: 3-D measurements: sketches of outer (top) and inner (bottom) absorbers showing the reference frame, scan lines, and the definitions for the geometrical variables.

# 4 Analysis of measurements on outer absorbers.

## 4.1 Thicknesses.

Fig. 7 shows all the thicknesses measured in all the M00 outer absorbers (except for two of them, for which we will have a particular discussion) as a function of the half-wave number (see Fig. 3 for numbering convention) and in histograms. The measurements at the acute and obtuse sides of the absorbers are shown separately in Fig. 7. Measurements from absorbers from the same mould have been given the same marker type.

It is apparent from Fig. 7 that there is a clear systematic in the thickness along the absorber edges, being this more pronounced in the obtuse side. One should notice that our thickness measurements are most affected by edge effects, and that the systematics is expected to be largely reduced (if not totally) if we measured in the middle of the absorber.

We understand the particular shapes of the thickness dependence with the half-wave number as follows: The absorber is sandwiched between the bottom and top pieces of the mould. View from a different point, the absorber acts as a "shim" between those parts. But the total surface of the mould ( which is under preassure in the autoclave) is larger than the area of the absorber inside and as the mould bottom and top parts are not fully rigid bodies [2], the zones of the mould outside the absorber contour are slightly deformed by the autoclave pressure (since in those zones there is no "shim" between both mould parts). These deformations translates into nonuniformities in the pressure applied by the mould parts on the absorber at its contour, and in particular at its obtuse and acute edges. The fact that the thickness systematics in the obtuse part is stronger is, under the above hypothesis, a reflection of the particular geometry of the absorber at this place (almost V shaped) which leaves more empty space between the bottom and top mould parts.

Nevertheless, even with these systematics, the RMS of all the thickness measurements made at the acute and obtuse absorber sides is 26 $\mu m$ and 33 $\mu m$, below the tolerance values of 110 $\mu m$ and 36 $\mu m$ respectively (see the histograms in Fig. 7).

In order to separate the thickness systematic from edge effects along the absorber sides, from the thickness reproducibility in a given point, we present in Fig. 8 the mean and RMS of all the measurements done in every half-wave surface as a function of its half-wave number. The thickness means follow nicely the shape already sketched by the data Fig. 7. The thickness RMS obtained in all the half-wave surfaces are always below 25 $\mu m$ and in most of the cases close to 15 $\mu m$.

Another way, mould wise, of having a look at the reproducibility of the absorber thickness is presented in Fig. 9 for the absorbers made in mould no. 2. We have chosen 4 half-wave surfaces at both acute and obtuse sides (those corresponding to the basic quality control), and plotted the measured thickness on them as a function of the number of autoclave cycle in which the absorber was produced. Very good reproducibilities are obtained with RMS typically below or around 10 $\mu m$. The only exception is half-wave no. 2 in the obtuse side (see Fig. 3 for its location within the absorber) with a significantly larger RMS. Notice that the zone where half-wave no. 2 is, seems to be most affected by the mould deformation discussed above (see Figs. 7 and 8). The same analysis in the rest of the moulds show similar features as those discussed here for mould no. 2.

### 4.1.1 The case of absorbers b047_10_m00c01 and bun01_08_m00c01

Two problems in moulds no. 10 and 8 respectively were detected from the analysis of the measurements performed on the corresponding absorbers after the first cycle.

The black squares in Fig. 10 show the thickness measurements from absorber b047_10_m00c01. Their dependence with the half-wave number is rather different than for the rest of the absorbers (see Figs. 7 or 8). In particular the thickness measured at the inside part (i.e. which will be closest to the ATLAS interaction point) are significantly larger. After a careful inspection of mould no. 10, we found in its top part that the flat surface which presses on the lateral-bar/absorber junction was around 0.5 $mm$ higher than its nominal height w.r.t. the absorber/mould symmetry plane. Therefore these 0.5 $mm$ acted as a shim preventing the rest of the top part be at nominal distance from the bottom part during the curing cycle. We brought this mould to the machine workshop for repair and after it, the absorbers from the rest of the cycles showed fully satisfactory thicknesses (see the rest of the measurements in Fig. 10).

We were worried about not finding this defect at the time of the quality control of the curing moulds. After carefully inspecting all our files, we realized that this mould part had sneakily avoided all our controls and measurements but that fortunately, it was the only one.

[2] To quantify this lack of rigidity, gravitational sagging in the mould in working conditions is of the order of 0.1 mm. But if we hold its bottom or top parts only by three extreme points, we have measured in the worst conditions up to several tenths of a millimeter.

A less important problem was found in the analysis of the data from bun01_08_m00c01. Fig. 11 shows this data (black squares) along with the measurements from the rest of the absorbers made in mould no. 8. Again there is a clear difference between the results at the inside part in the obtuse side of bun01_08_m00c01 and the corresponding measurements at the rest of the absorbers. (see also Figs. 7 or 8 for measurements at absorbers from moulds different than no. 8). This time it was noticed that one of the six telescopic stoppers which are located at the contour of the bottom part of the mould in order to reduce the mould deformations discussed in 4.1 was not adjusted as in the rest of the moulds. After proper adjustment, the rest of the absorbers from that mould didn't show that effect any more (see the rest of the measurements in 11).

We think that the effects on the global quality of the absorber from this second type of mould problem is very small and it only affects the absorber edges.

We observe in essentially all moulds the tendency of slight thickness reduction with the number of cycle (i.e. with the amount of time in which the moulds have been under pressure), see Fig. 12. The effect is more apparent in the obtuse side. This may be an indication of a stopper disadjusting affecting to most of the stoppers. We will check the stoppers before starting M01.

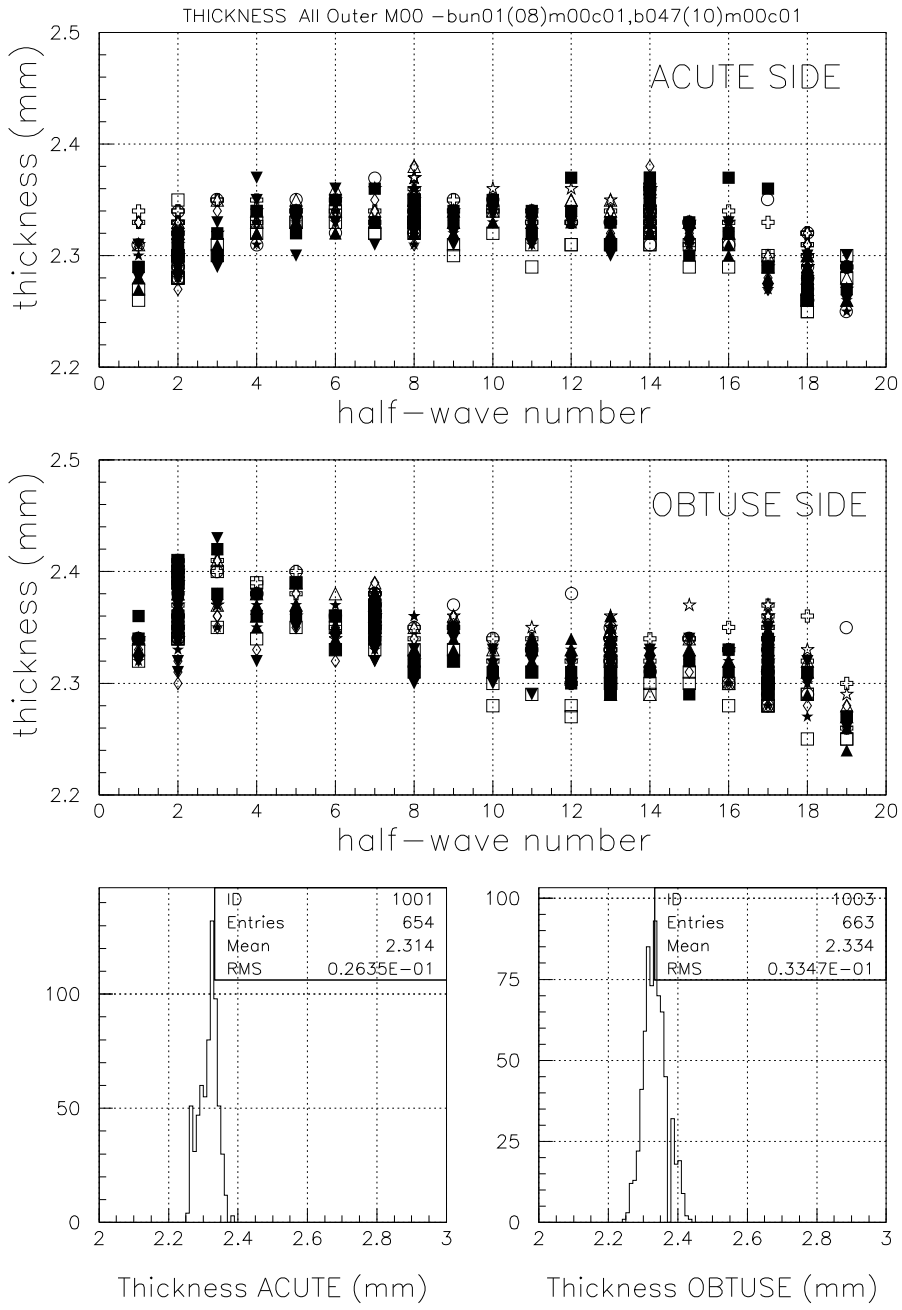


Figure 7: Thicknesses measured at the acute and obtuse sides of all the outer absorbers produced for M00 (except the two indicated in the figure's title) as a function of the number of the half-wave surface where the thickness was actually measured (top and middle plots). Measurements from absorbers from the same mould have been given the same marker type. Bottom plots: histograms for all these thicknesses measured. The tolerances for the thickness RMS are 0.110 *mm* in the acute side and 0.036 *mm* in the obtuse side.

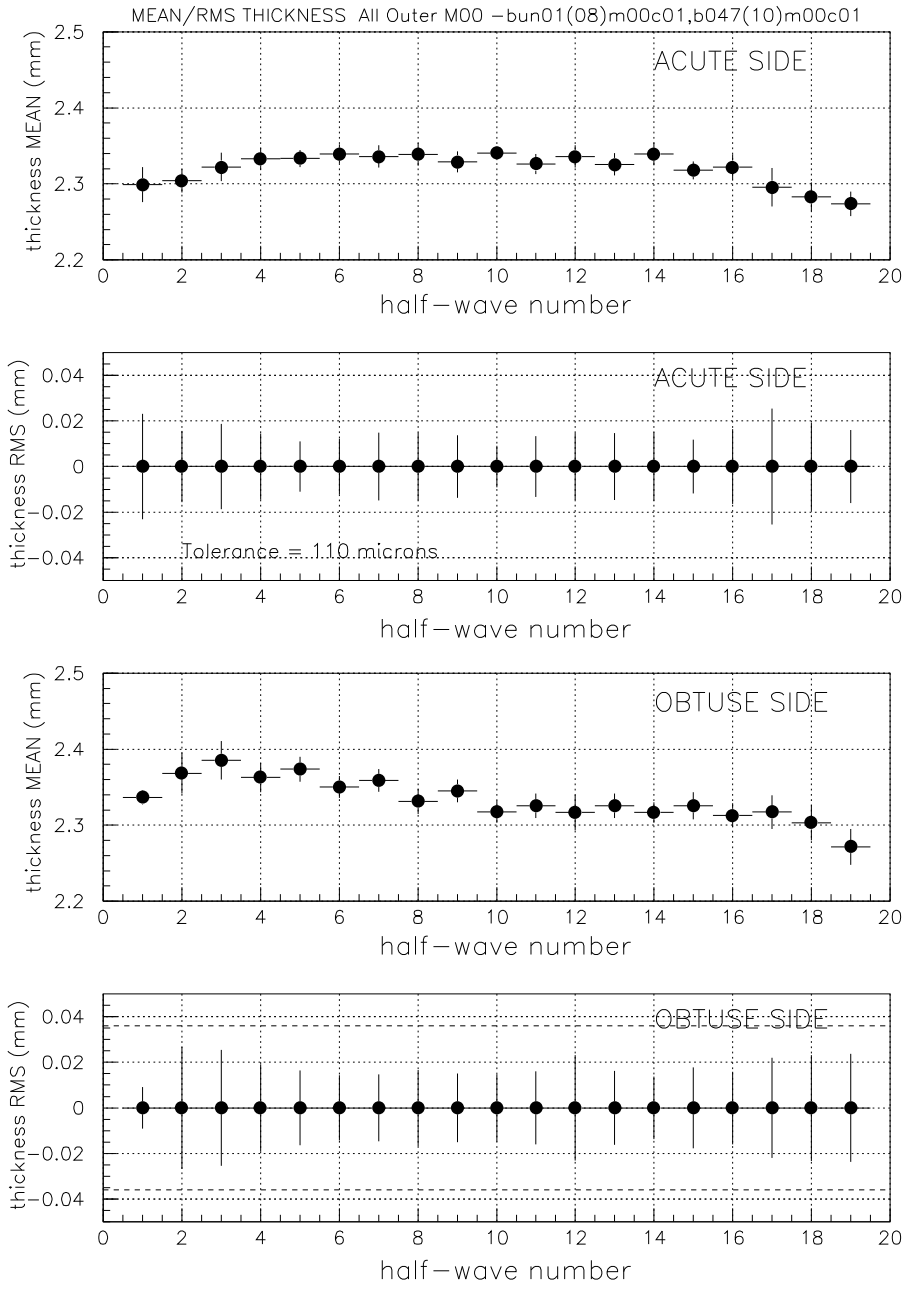


Figure 8: Mean and RMS of all the thicknesses measured in a given half-wave surface as a function of its number. The results from all the M00 outer absorbers produced, except the two indicated in the figure's title, have been included. In the RMS plots, the results are shown as error bars on points set at 0. These error bars are the same as those in the plots for the mean. The tolerances for the RMS in the obtuse side are indicated by two dashed lines.

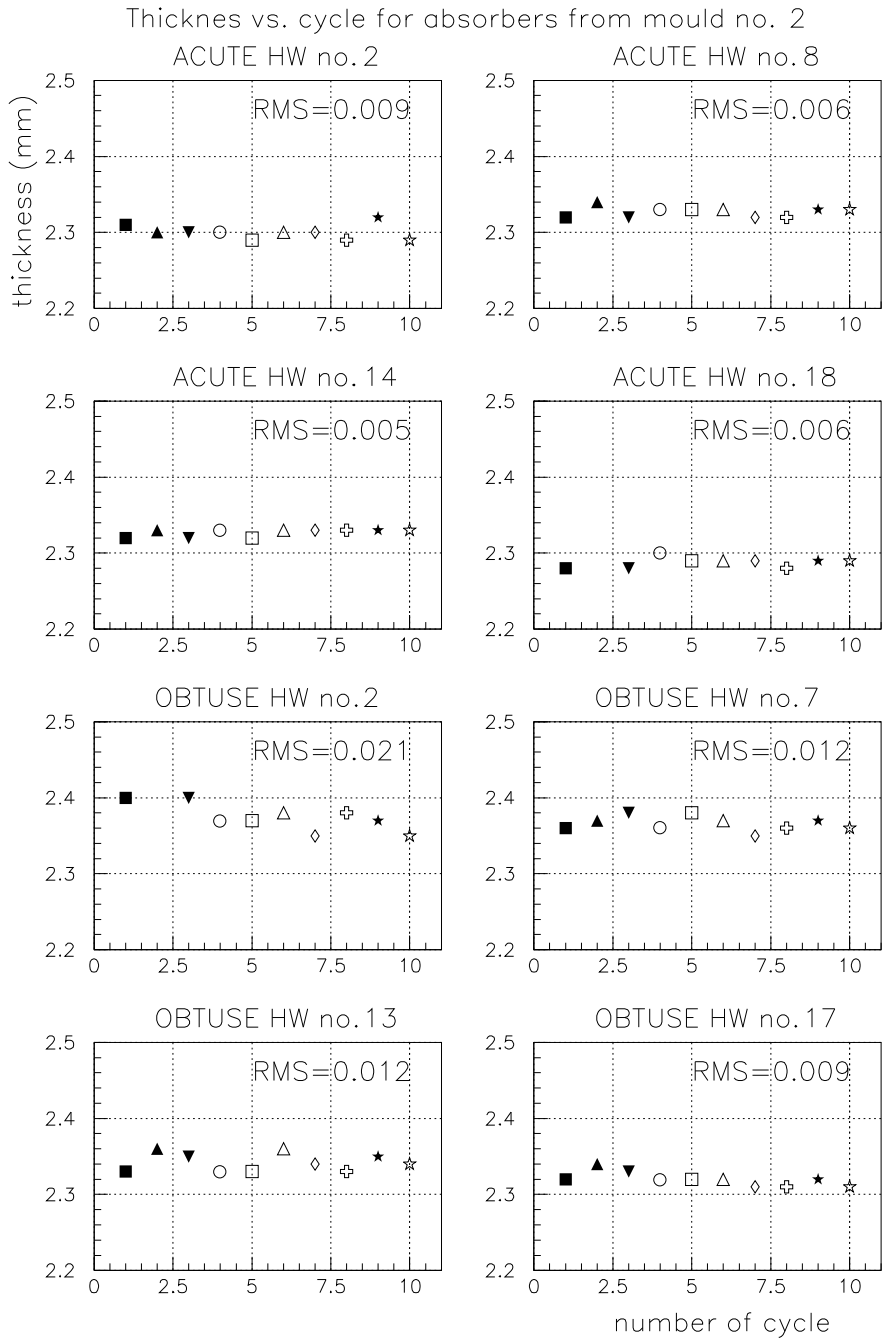


Figure 9: Outer absorbers made at mould no. 2: thicknesses measured in 4 fixed half-wave surfaces at both, acute and obtuse sides, as a function of the number of the cycle in which the particular absorber was produced.

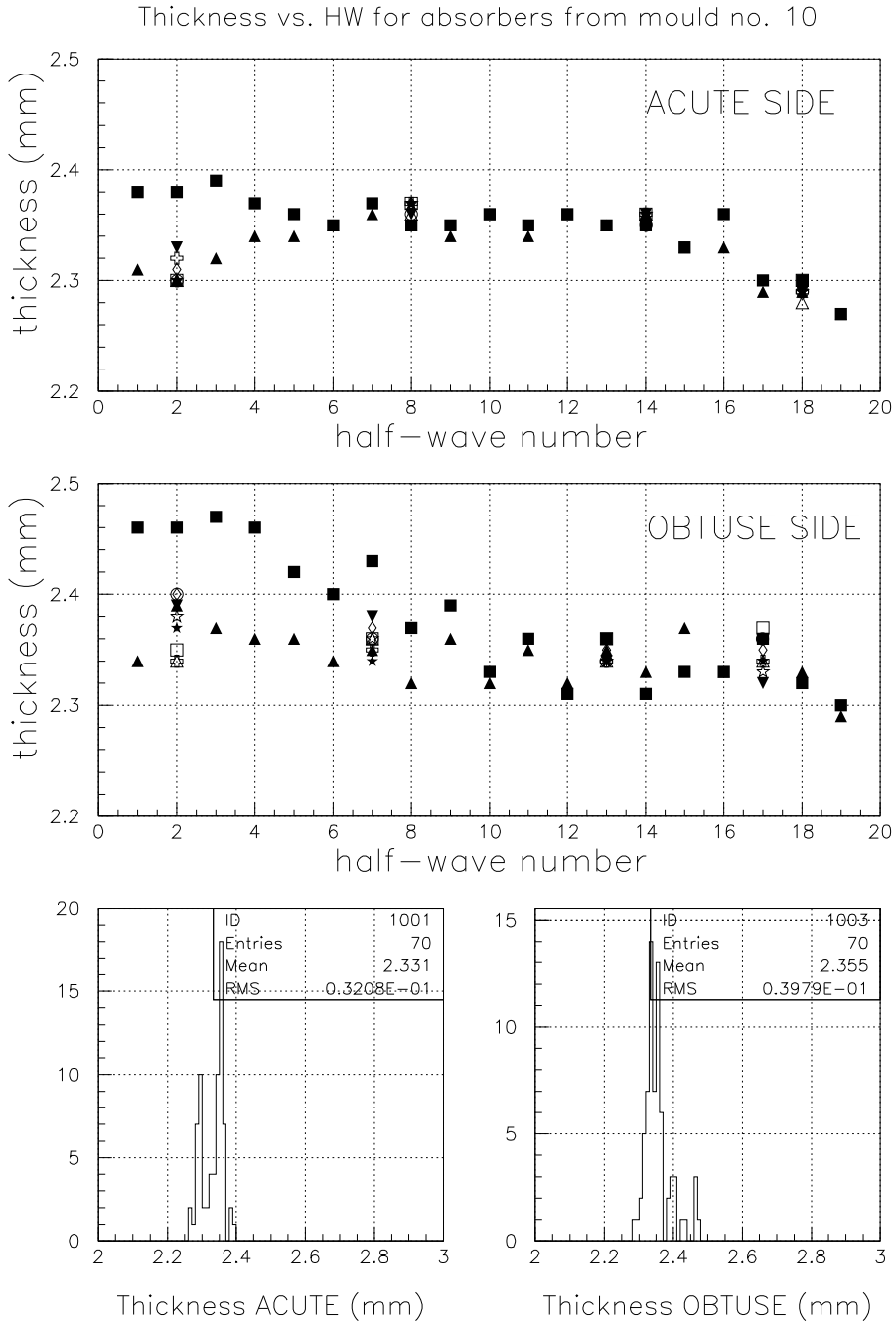


Figure 10: Outer absorbers made at mould no. 10; measured thickness vs. half-wave number. The black squares are the results of the thickness measurements on b047_10_m00c01 (first cycle). The rest of the markers correspond to measurements done in the absorbers from cycles 2 to 10. In particular the black up-triangles are from absorber b076_10_m00c02 (second cycle). Bottom plots: histograms for all these thicknesses measured.

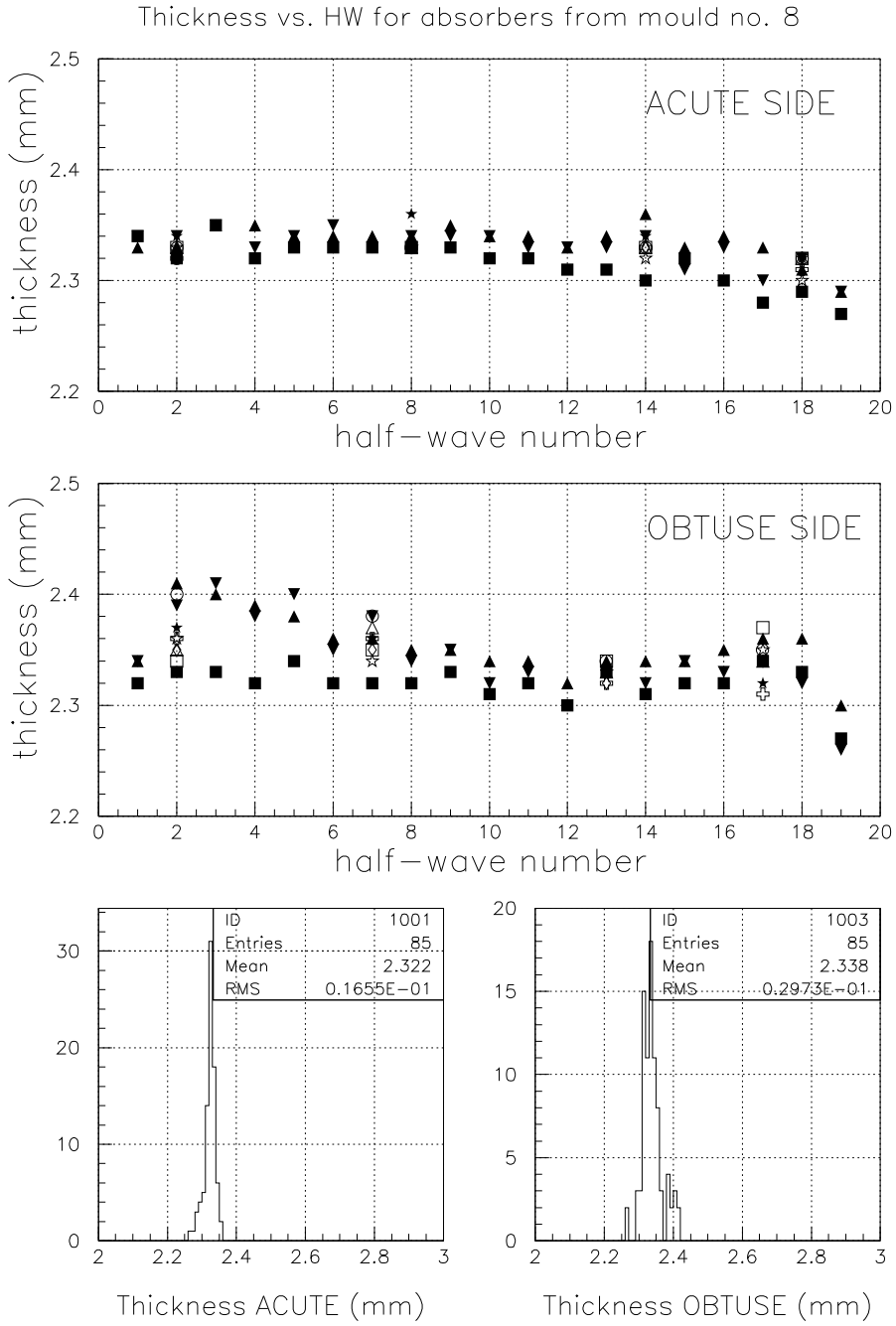


Figure 11: Absorbers made at mould no. 8; measured thickness vs. half-wave number. The black squares are the results of the thickness measurements on bun01_08_m00c01 (first cycle). The rest of the markers correspond to measurements done in the absorbers from cycles 2 to 10. In particular the black up-triangles are from absorber b070a_08_m00c02 (second cycle). Bottom plots: histograms for all these thicknesses measured.

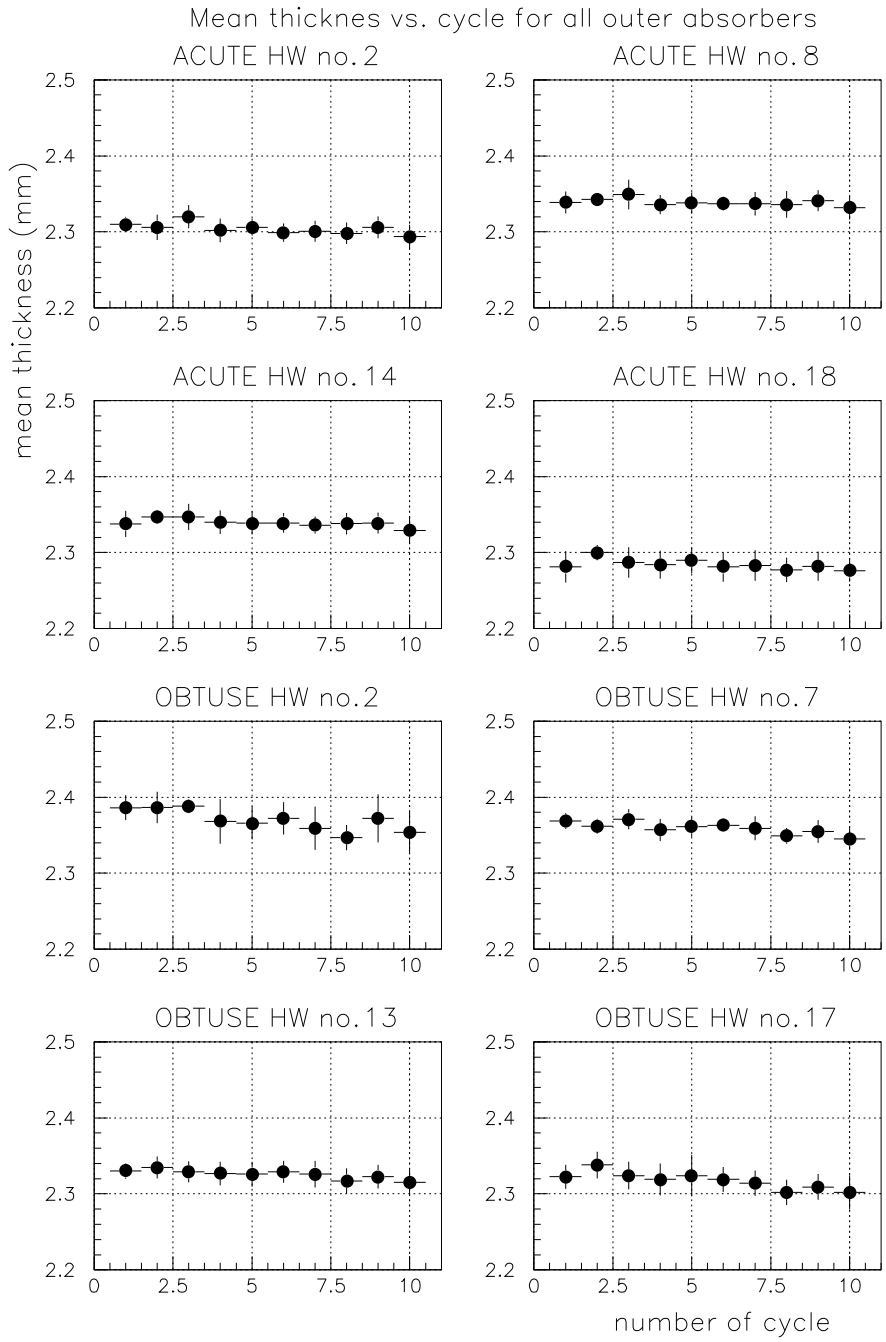


Figure 12: Mean thickness of all M00 outer absorbers as a function of the number of the cycle in which the absorbers were produced for 4 fixed half-wave surfaces at both, acute and obtuse sides. The error bars are the corresponding RMS's.

## 4.2 Angles of the half-wave surfaces.

Fig. 13 show the deviations w.r.t. nominal of the measured half-wave surface's angle as a function of the half-wave no. and at the eight scan lines. Notice that the lowest Y value corresponds to the obtuse side of the absorber whereas the highest Y value is at its acute side. See Fig. 6 for reference frame. Data from all the 3D measured M00 outer absorbers are shown. Absorbers from the same mould are given the same marker type.

For the sake of completeness we have also included in Fig. 13 the measurements at half wave surfaces no. 1 and 19 despite of their much worse angular measurement resolution as discussed in sec. 3.2.

Several features are already apparent in Fig. 13:

1. The measured $\beta$ angles are in general larger (in absolute value) than nominal, i.e. the produced absorbers have acuter folds, see Fig. 6, than designed. As the curing moulds were measured to have very precisely machined folds ( with angles to better than 0.3 mr, see [4]), the acuter folds are believed to be a reflection of a global absorber transversal shrinkage. This shrinkage has been observed in all the accordion prototypes made so far.

2. There is a clear jitter in the measured angles which starts in the external side of the absorber (w.r.t. the ATLAS IP, large half-wave surface no.) at the obtuse side (low Y) and propagates to the internal side as we move towards the acute absorber side. The source of this jitter is not yet known. This and the previous systematic effects are better seen in Fig. 15 (see below for details).

3. One can appreciate how the results from b047_10_m00c01 (stars) separate clearly from the cloud formed by all the measurements mainly at the obtuse-internal absorber region (low half-wave and Y numbers).

4. Also the results from bun01_08_m00c01 (open crosses) deviate from the general trend. In this case the effect is mainly at the obtuse-external absorber region.

Fig. 14 shows the distributions for the deviations w.r.t. nominal of all the measured half-wave surface's angles at the eight scan lines. Here neither the data from b047_10_m00c01 nor the measurements at half-wave nos. 1 and 19 have been included. The RMS tolerances are given in radians; they vary longitudinally as the LArg. gap does (see [2]). The measured R.M.S.'s are well within tolerances except in the most obtuse scan line where it is marginally above the specs. established in sec. 2.3. Their typical value is 2.4 milliradians. Therefore the systematic angular jitter commented above is small enough not to put in jeopardy the quality, in terms of geometry, of the absorbers. The mean deviation w.r.t. nominal of the measured angles is around 2.2 milliradians increasing slightly when moving from the obtuse to the acute absorbers sides.

In order to separate systematic effects from the reproducibility in a given point, we present in Figs. 15 and 16 the mean and RMS of all the measurements (always w.r.t. nominal) from every half-wave surface as a function of its half-wave number and at the eight scan lines. The evolution of the angle jitter discussed above appears extremely clear in Fig. 15. The angle RMS obtained point-to-point are well below tolerances except a couple of cases showing a marginal excess. In most of the the half-wave surfaces, angular reproducibilities around or below 1 milliradian are achieved.

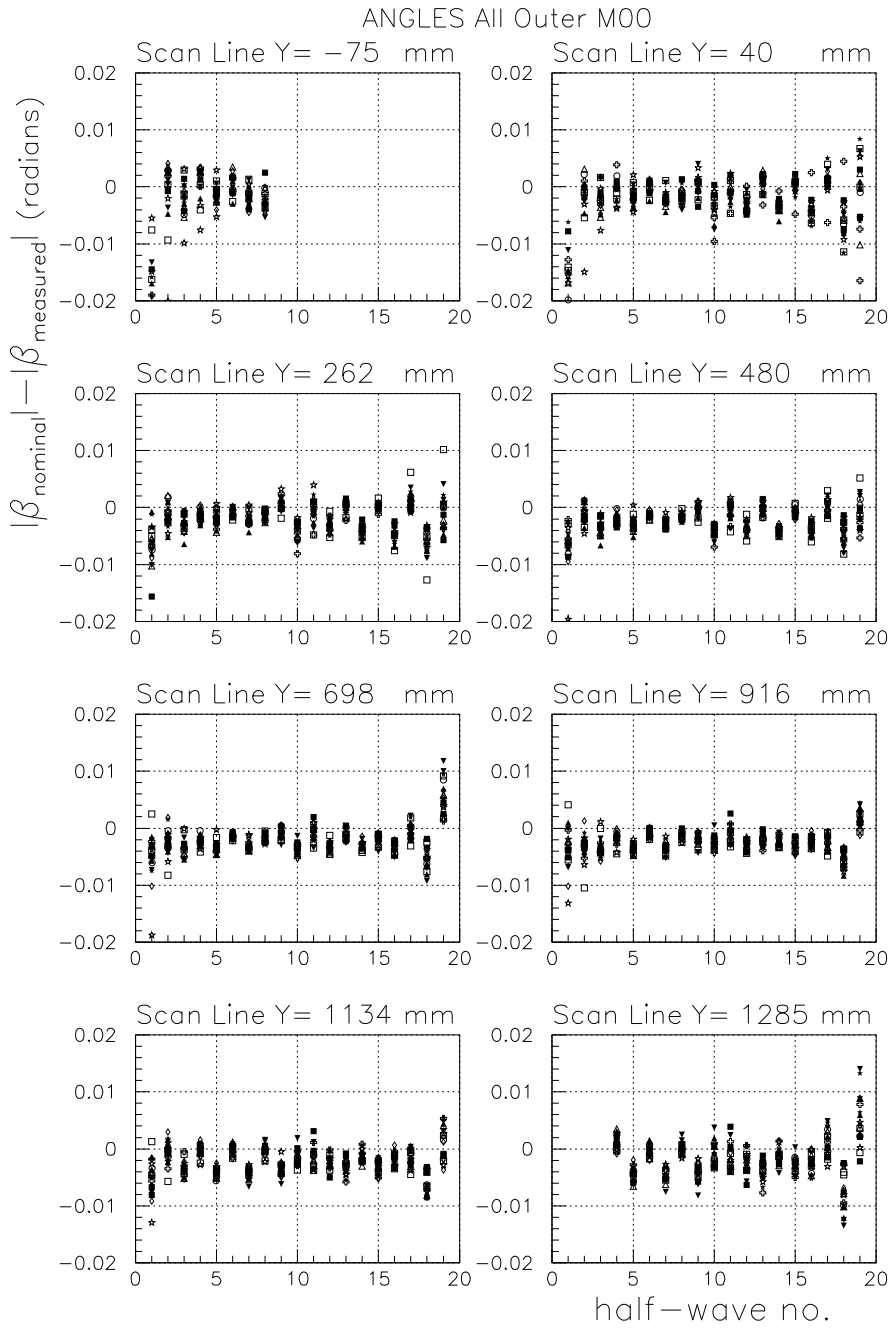


Figure 13: Deviations w.r.t. nominal of the measured half-wave surface's angle as a function of the half-wave no. and at the eight scan lines. Data from all the 3D measured M00 outer absorbers are shown. Absorbers from the same mould are given the same marker type. The lowest Y value is at the obtuse side of the absorber; the highest Y value is at its acute side.

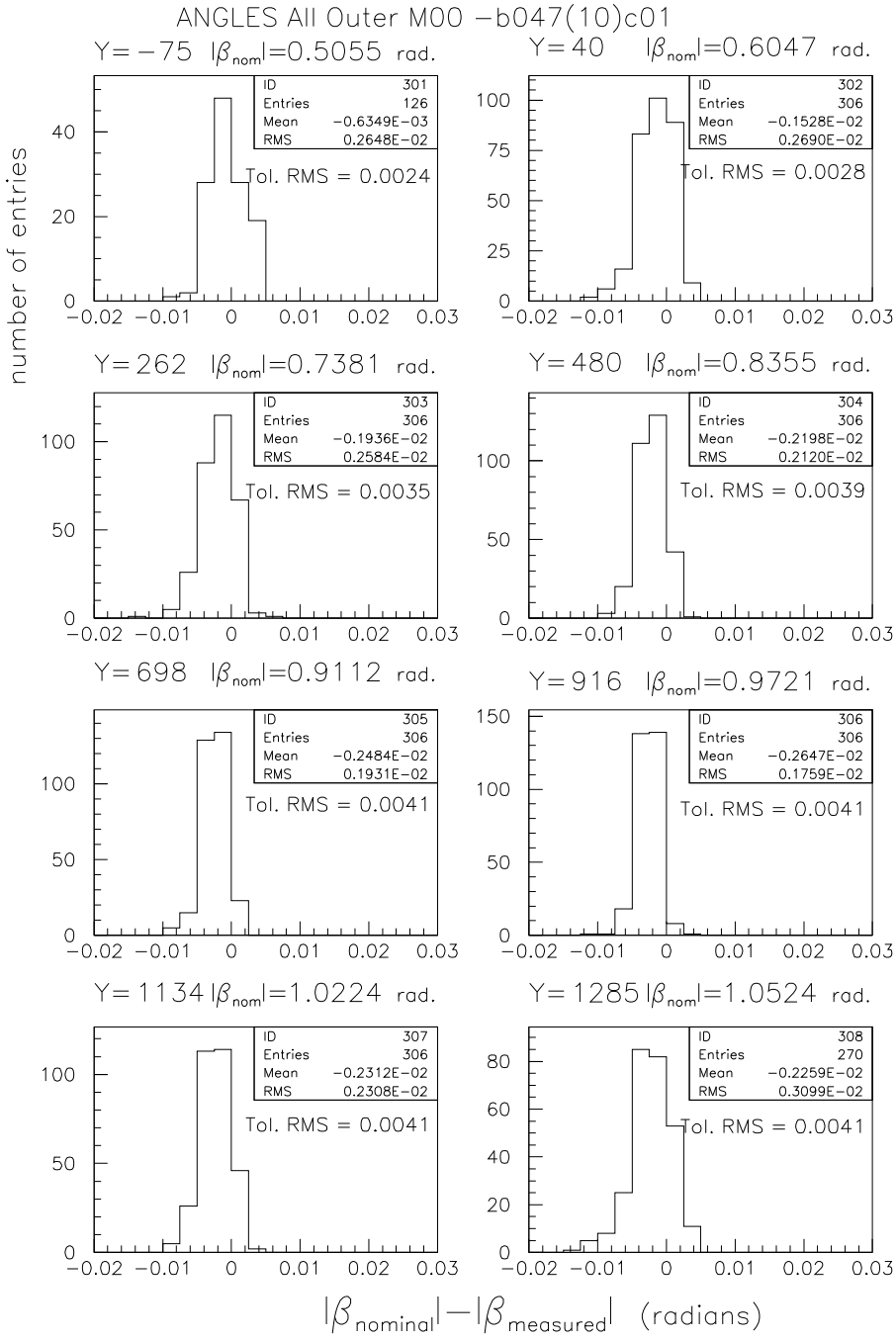


Figure 14: Histograms for the deviations w.r.t. nominal of the measured half-wave surface's angle at the eight scan lines. Data from all the 3D measured M00 outer absorbers (except b047_10_m00c01) are shown. The RMS tolerances are given in radians. The lowest Y value is at the obtuse side of the absorber; the highest Y value is at its acute side.

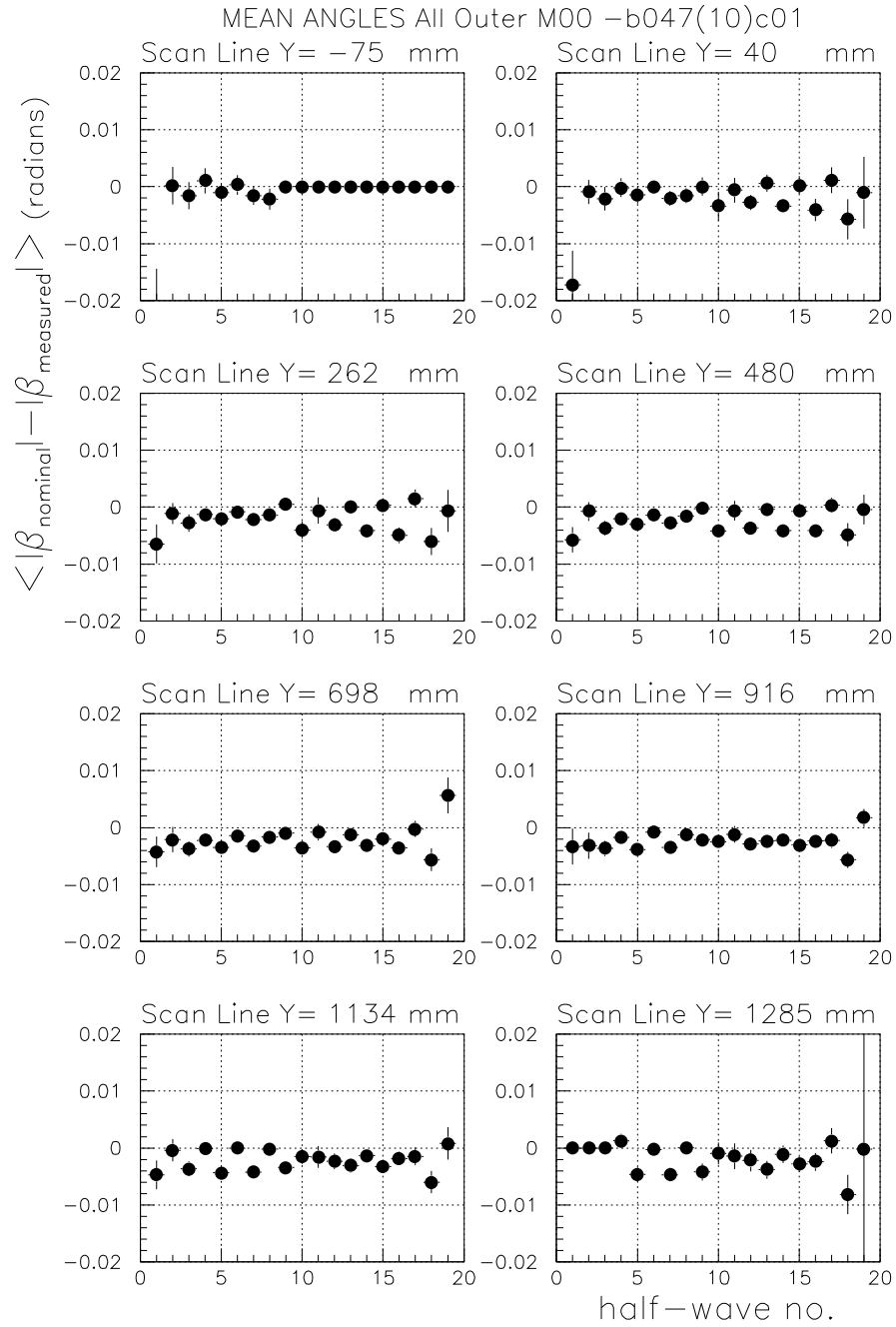


Figure 15: Mean of the deviations w.r.t. nominal of the measured half-wave surface's angle as a function of the half-wave no. and at the eight scan lines. All the 3D measured M00 outer absorbers (except b047_10_m00c01) are included in the mean calculation. The error bars are the RMS. The lowest Y value is at the obtuse side of the absorber; the highest Y value is at its acute side.

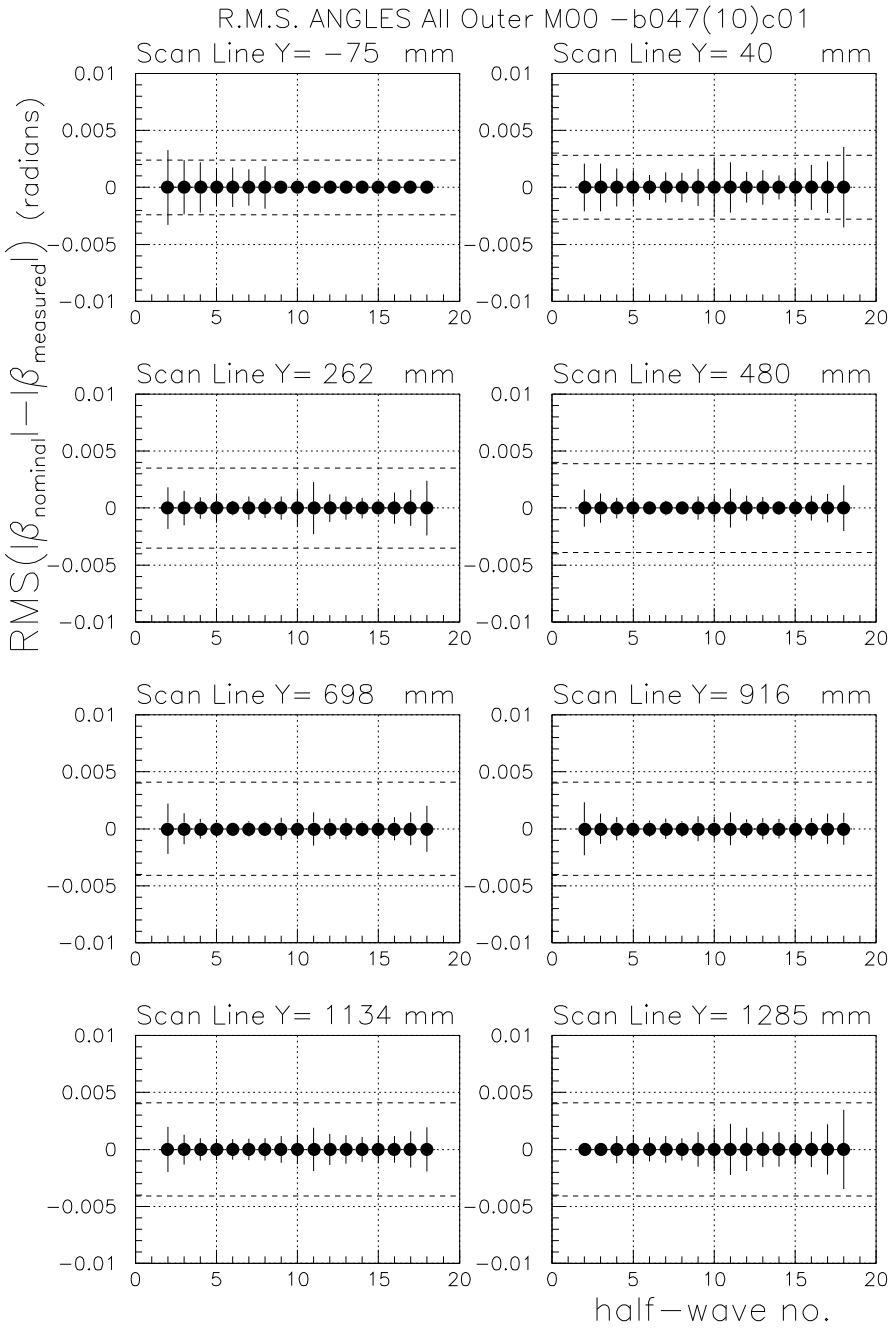


Figure 16: R.M.S. of the deviations w.r.t. nominal of the measured half-wave surface's angle as a function of the half-wave no. and at the eight scan lines. All the 3D measured M00 outer absorbers (except b047_10_m00c01) are included in the mean calculation. The data are shown as error bars on points at 0. The dashed line indicate the tolerances. The lowest Y value is at the obtuse side of the absorber; the highest Y value is at its acute side.

## 4.3 Fold's coordinates.

In this subsection we study the reconstructed X and Z coordinates of the absorber fold's along the six lines where a full transverse scan was carried out. See Fig. 6 for details of the reconstruction method.

Fig. 17 show the deviations w.r.t. nominal of the measured X coordinate of the folds as a function of the fold no. for the six scan lines. Data from all the 3D measured M00 outer absorbers are shown. It is apparent the absorber shrinkage that we envisaged when analyzing the angles. The magnitude of the shrinkage increases almost linearly with Y. There is no absorber deviating clearly from the rest, except maybe, the famous b047_10_m00c01.

In order to separate systematic effects from the reproducibility in a given point, we present in Fig. 18 the mean and R.M.S. of all the X measurements (always w.r.t. nominal) from every fold as a function of its fold number and at the six scan lines. From the plots for the means we estimate a shrinkage of approximately 1.3 (0.3) mm at the acute (obtuse) side. The R.M.S. of the measurements from all absorbers in a given fold position are typically 50 (100) $\mu m$ in the obtuse (acute) sides, within tolerances in all the cases.

Notice that the reference frame is such that X=0 would correspond approximately to a fold no. 20. The fact that the dispersion of the measurements is larger at the folds close to the internal side of the absorber (low no. of fold) is a reflection of the particular choice of the X=0 position since deviations from nominal are accumulative effects from fold to fold and locally, the distance along the X axis between adjacent folds is expected to show similar dispersions independently of the position of the fold (see Fig. 19 for the distribution of the distance in X between adjacent folds at the different scan lines; their R.M.S.'s are similar to the R.M.S. for the fold closest to X=0, fold no. 18, in Fig. 18). As a result, if, for example, we had chosen the X=0 at fold no. 9, we would expect the measured RMS at folds no. 3 (18) to be smaller (larger) than those in Fig. 18 by a factor $1/\sqrt{2}$ (2).

Fig. 20 show the deviations w.r.t. nominal of the measured Z coordinate of the folds as a function of the fold no. for the six scan lines. Data from all the 3D measured M00 outer absorbers are shown. The following features are apparent:

1. It seems that the absorbers come out of the mold with a small but significant twist with the inside part of the absorber deformed upwards (in the reference frame sketched in Fig. 6) about 0.5 mm at its maximum. This and other global systematic effects are better seen in Fig. 21 (see below for explanation of the contents in Fig. 21).

2. The particular shape of the twist seen in Fig. 20 may be forced by the local constrains imposed by the measuring jig (recall that in the jig the acute side of the absorber was effectively free, see subsec. 3.2).

3. At the internal side (low no. of fold) of the most obtuse scan line, the dispersion of the measurements becomes large. We are not sure of the source of this effect, but we think it is a mixture of a not proper absorber fixation to the jig and small deformations of the longitudinal internal bars in their thinest part. With respect to the former, we believe the direction of the corresponding positioning pin is not properly defined by the jig due to a large clearance of the pass-through hole (see subsec. 3.2).

4. Three absorbers show results that differ from the bulk: b050_01_m00c01 (the most top full squares), bun01_08_m00c01 (empty crosses) and b027_07_m00c07 (top most empty diamonds). The case of bun01_08_m00c01 has been already discussed; its particular behavior at the most obtuse external side is a reflection of the corresponding angular behavior observed in Fig. 14. The reason for the behavior of the other two absorbers is not clear as it will be discussed later in this section.

Fig. 21 shows the mean and R.M.S. of all the Z measurements (always w.r.t. nominal) from every fold as a function of its fold number and at the six scan lines. The data from b050_01_m00c01, bun01_08_m00c01 and b021_07_m00c07 is not included in the calculations. The effects discussed above are clearly seen either in the plots for the means or those for the RMS. Except in the most obtuse scan line, the local dispersions (typically 75 $\mu m$ RMS) are reasonable well within tolerances. In the plot for the means a clear point to point jitter is apparent. This jitter is just an artifact of the Z reconstruction method which appears if the absorber has shrunk w.r.t. its nominal size due to an overall reduction of its fold's angles. Notice that the jitter is smaller in the obtuse side than in the acute as expected from the type of shrinkage established in subsec. 4.2.

### 4.3.1 The case of absorbers b021_07_m00c07 and b050_01_m00c01.

Fig. 22 shows the thicknesses, angles and X and Z coordinates measured in all the absorbers cured in mould 07 (where b021_07_m00c07 was produced). The large difference between absorbers appears only in the Z

coordinates. The shape of the difference may provide us with a key for the source of the problem: in the acute side (high Y) the measurements tend to converge both in the external and internal sides of the absorber (high and low fold number respectively), whereas for the rest of the absorber the convergence is only at the external side, being the discrepancy at the internal side largest in the middle part of the absorber (Y=480 mm). This fact, along with the observation of good reproducibility in the other variables measured (also the width, see next section, of b021 is very similar to the rest of the absorbers), may be an indication of an incorrect absorber positioning in the jig at the middle part of the internal longitudinal bar. Unfortunately we are not able to prove this hypothesis, the only thing we can do is to keep an eye on the next absorbers coming out from that mould.

A similar vague conclusion we arrived to after the analysis of the absorbers from mould 01 (see Fig. 23). There is no clear indication of any isolated effect producing the different Z behavior from the middle to the acute absorber part.

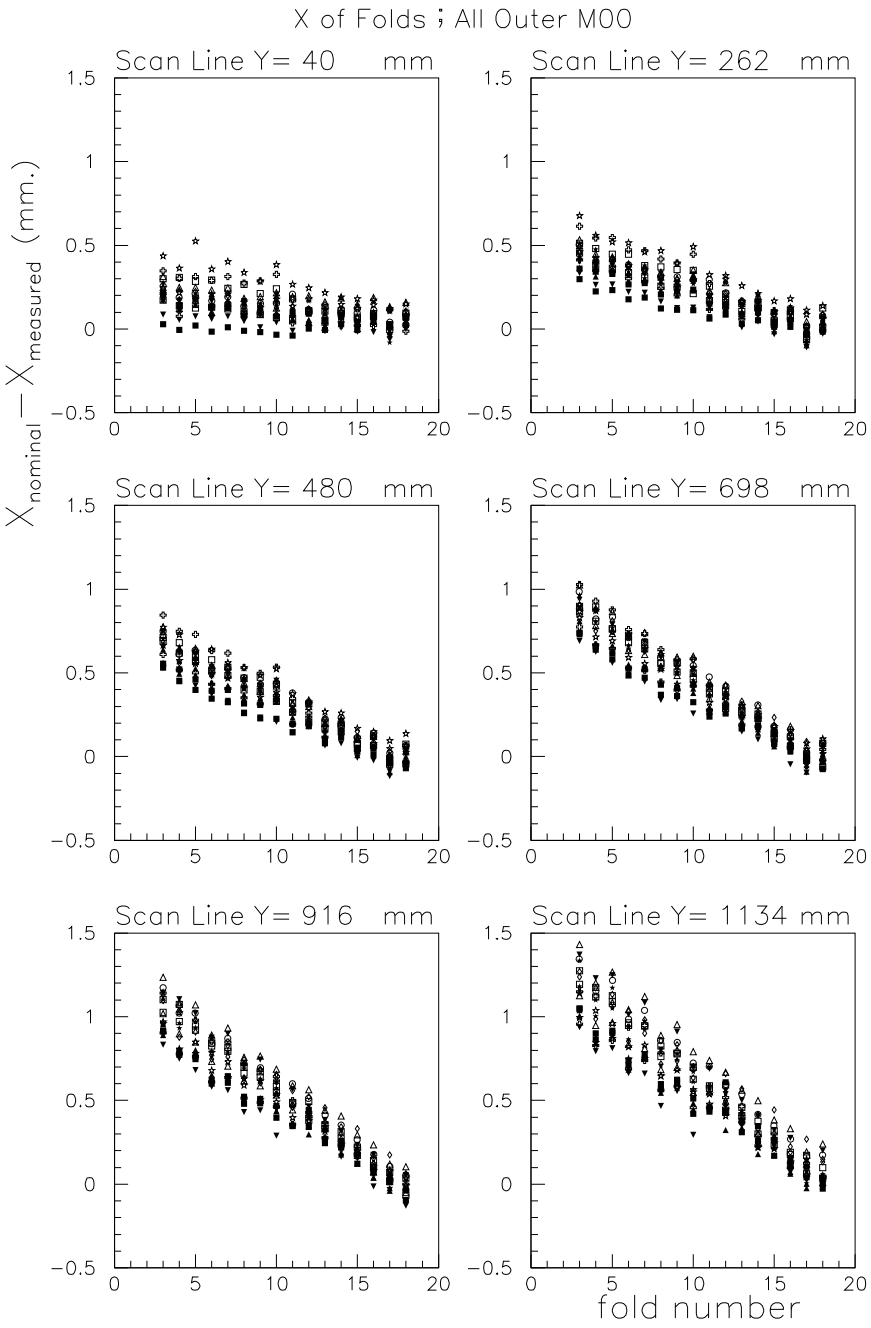


Figure 17: Deviations w.r.t. nominal of the measured X coordinate of the folds as a function of the fold no. and at six scan lines. Data from all the 3D measured M00 outer absorbers are shown. Absorbers from the same mould are given the same marker type. The lowest Y value is close to the obtuse side of the absorber; the highest Y value is close to its acute side.

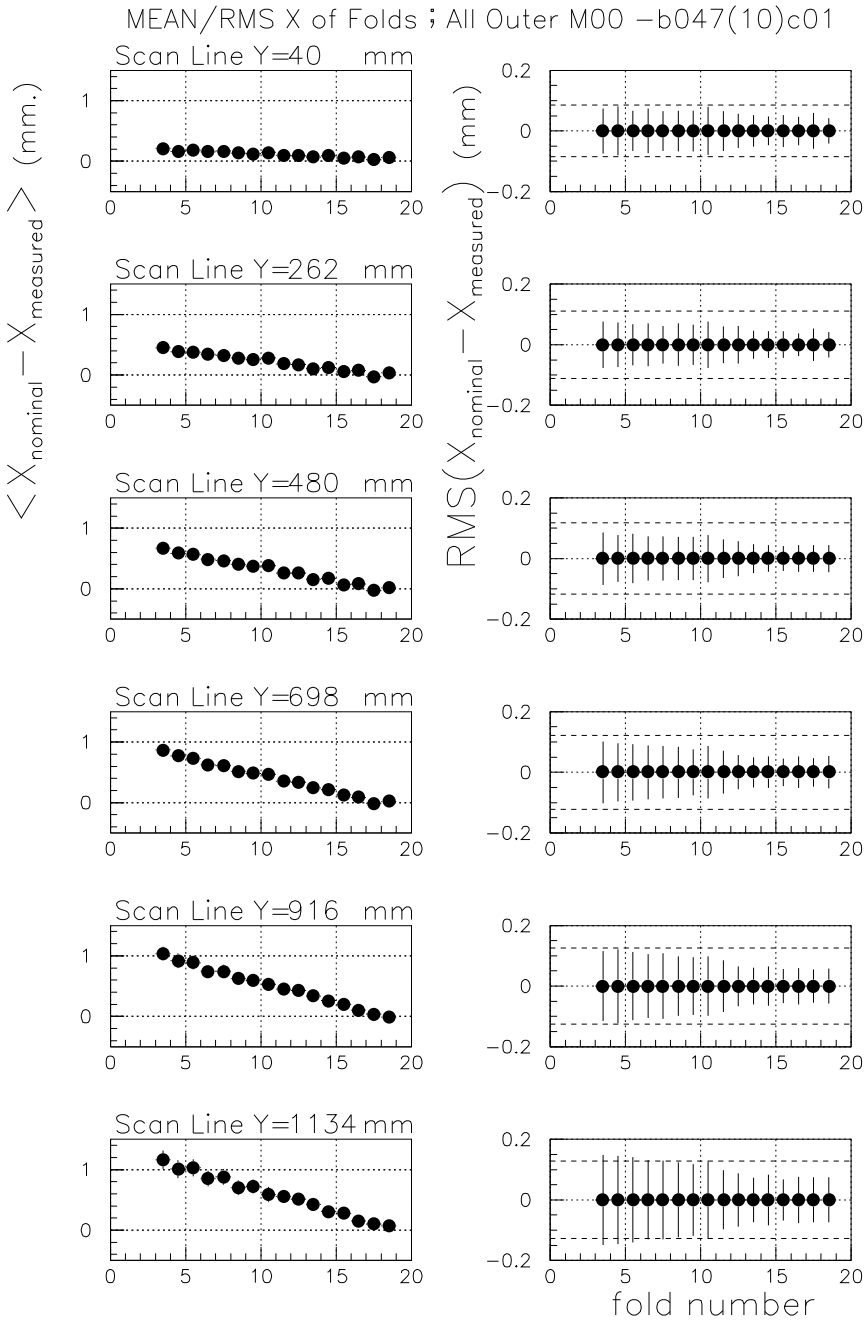


Figure 18: Mean and R.M.S. of the deviations w.r.t. nominal of the measured X coordinate in a given fold position as a function of its number and at six scan lines. Data from all the 3D measured M00 outer absorbers (except b047_10_m00c01) are shown. The R.M.S. results are shown as error bars on points at 0. These error bars are the same as those in the plots for the mean. The tolerances for the RMS are indicated by the dashed lines. The lowest Y value is close to the obtuse side of the absorber; the highest Y value is close to its acute side.

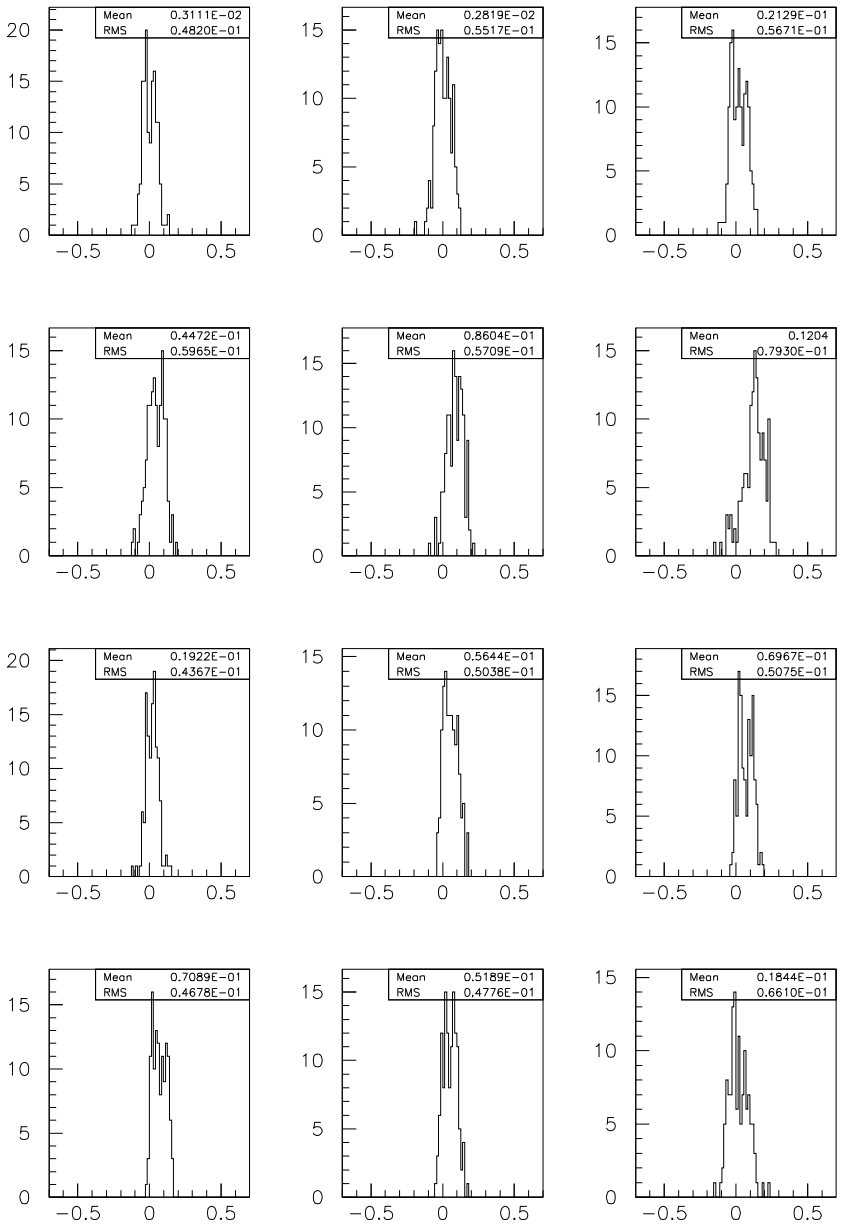


Figure 19: Deviations w.r.t. nominal of the measured distance in X between a bottom fold and its previous top fold (top six histograms) and between a top fold ant its previous bottom fold (bottom six histograms) for the folds at the six scan lines (one histogram per scan line). Bottom and top correspond to negative and positive Z respectively. The first (last) histogram of each group of six correspond to the scan line at the obtuse (acute) side. Data from all the 3D measured M00 outer absorbers (except b047_10_m00c01) are shown.

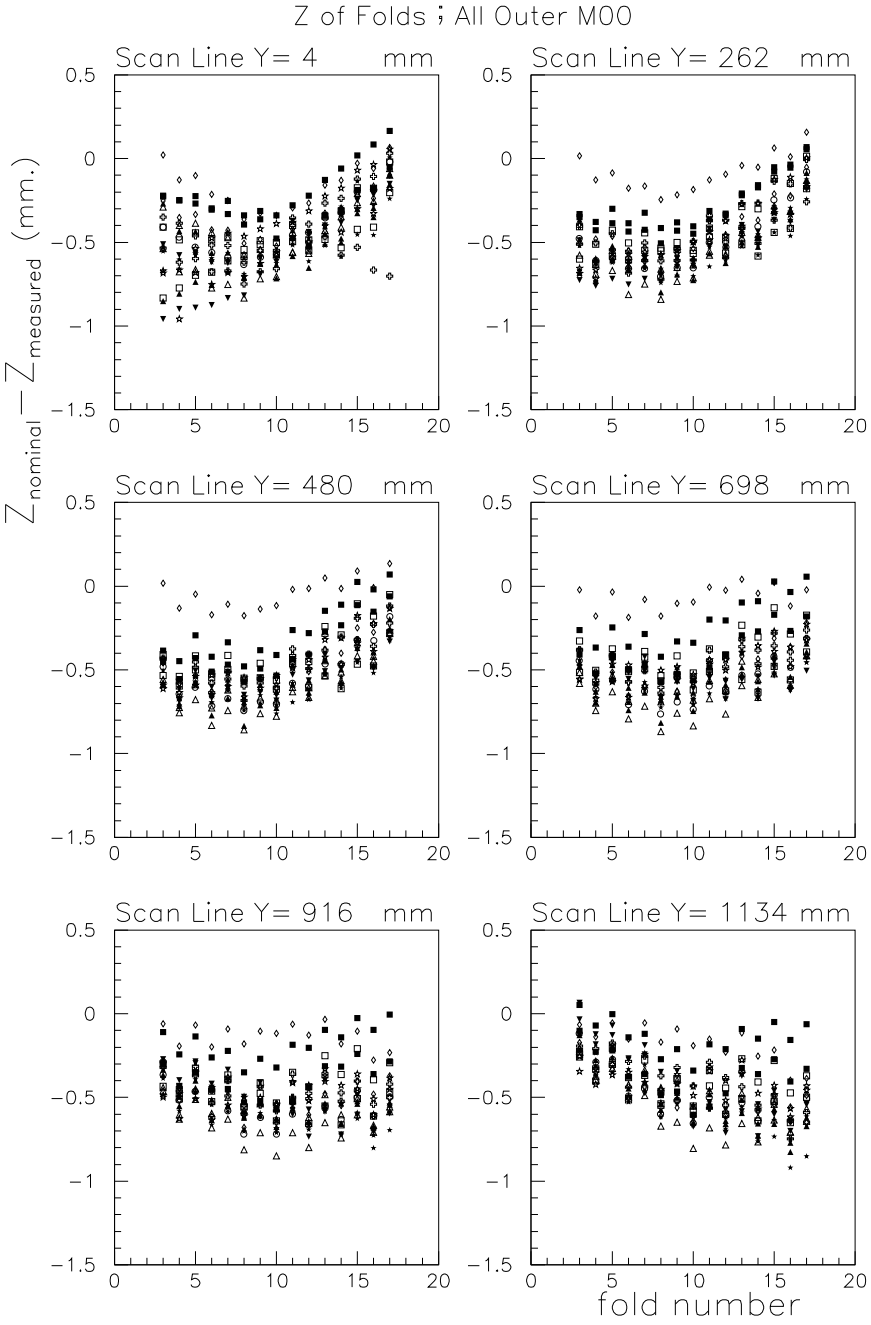


Figure 20: Deviations w.r.t. nominal of the measured Z coordinate at the folds as a function of the fold no. and at six scan lines. Data from all the 3D measured M00 outer absorbers are shown. Absorbers from the same mould are given the same marker type. The lowest Y value is close to the obtuse side of the absorber; the highest Y value is close to its acute side.

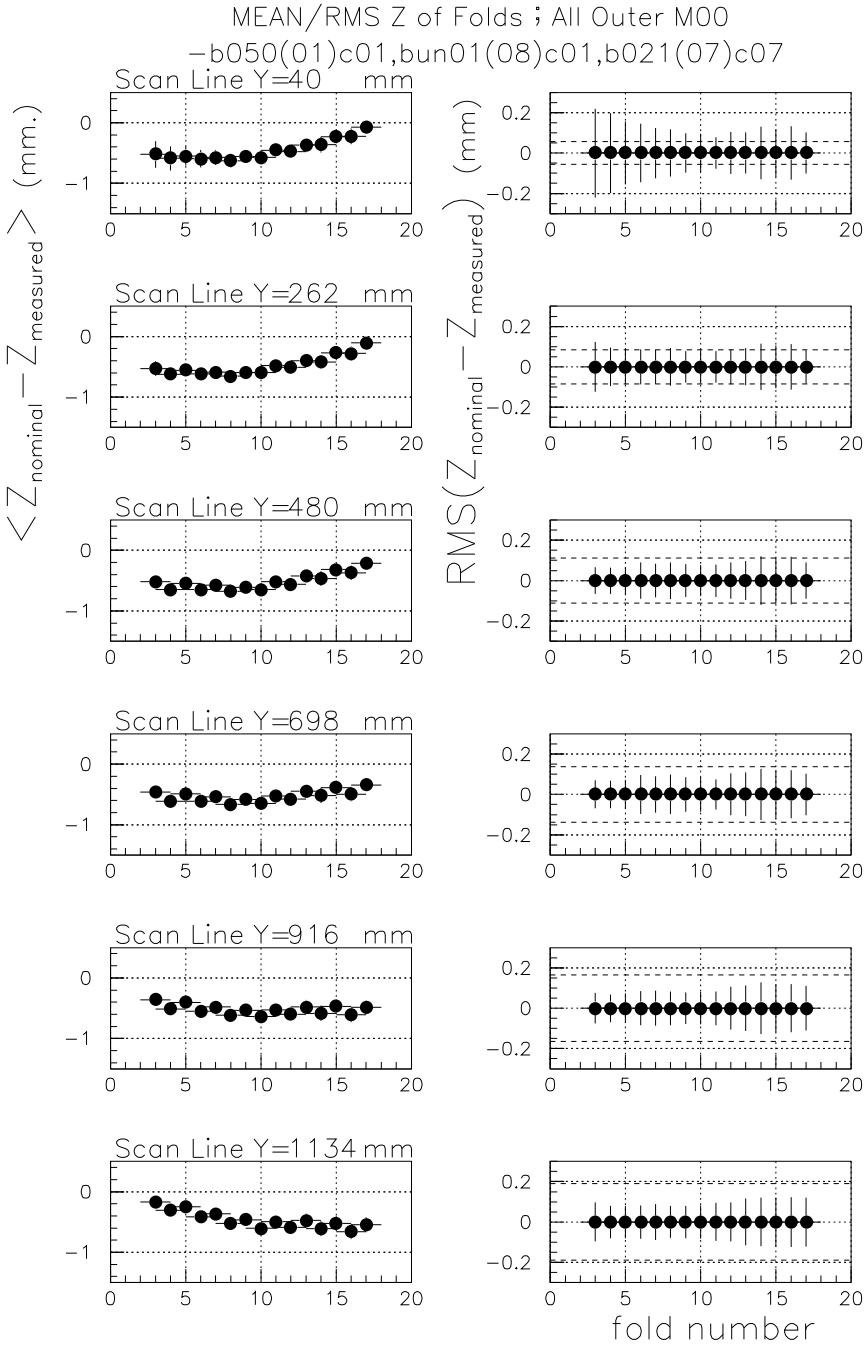


Figure 21: Mean and R.M.S. of the deviations w.r.t. nominal of the measured Z coordinate in a given fold position as a function of its number and at six scan lines. Data from all the 3D measured M00 outer absorbers (except b050_01_m00c01, bun01_08_m00c01 and b027_07_m00c07) are shown. The R.M.S. results are shown as error bars on points at 0. These error bars are the same as those in the plots for the mean. The tolerances for the RMS are indicated by the dashed lines. The lowest Y value is close to the obtuse side of the absorber; the highest Y value is close to its acute side.

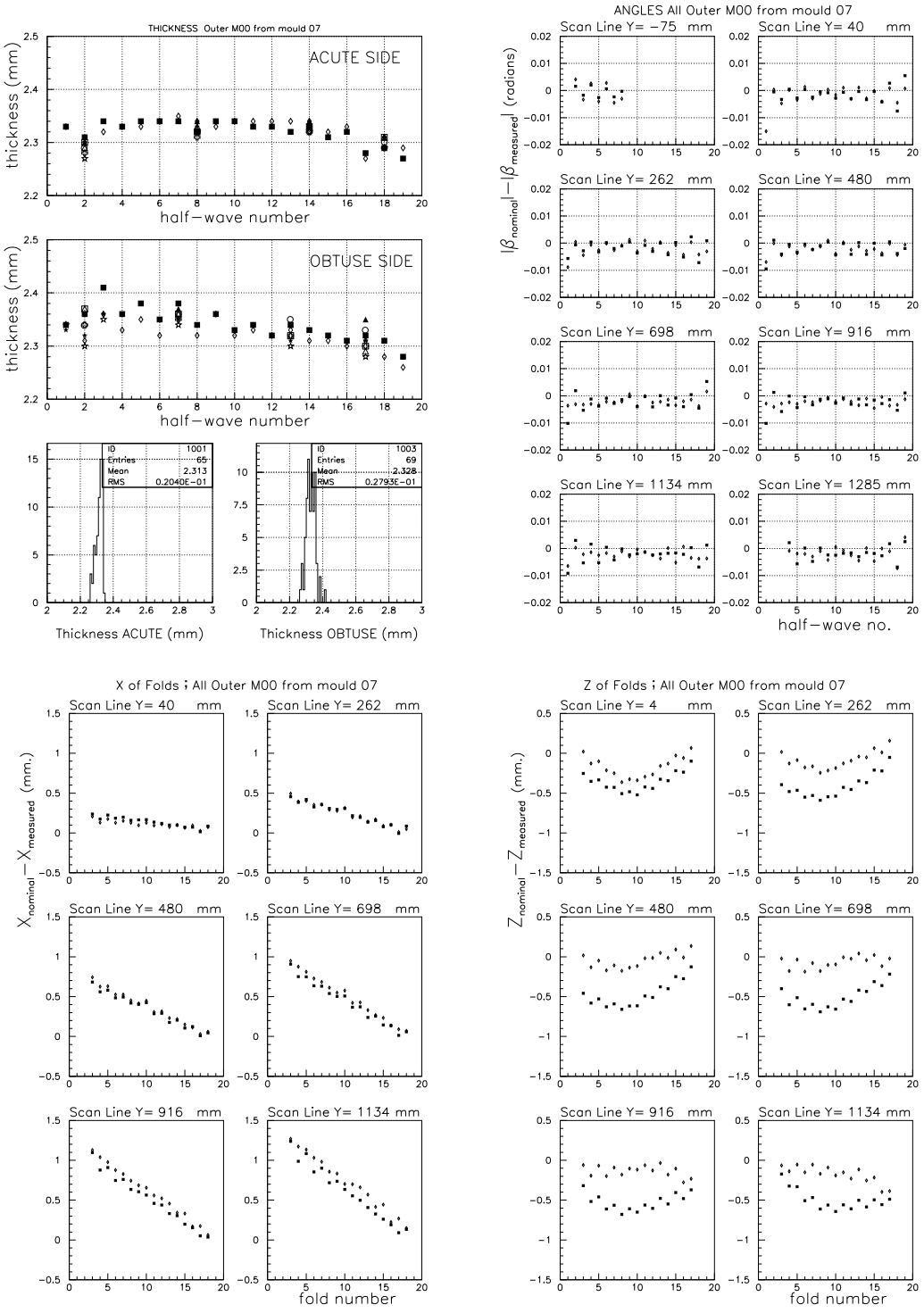


Figure 22: Thickness, angles and X and Z coordinate results from the measured absorbers cured in mould no. 7. The empty diamond correspond always to b021_07_m00c07.

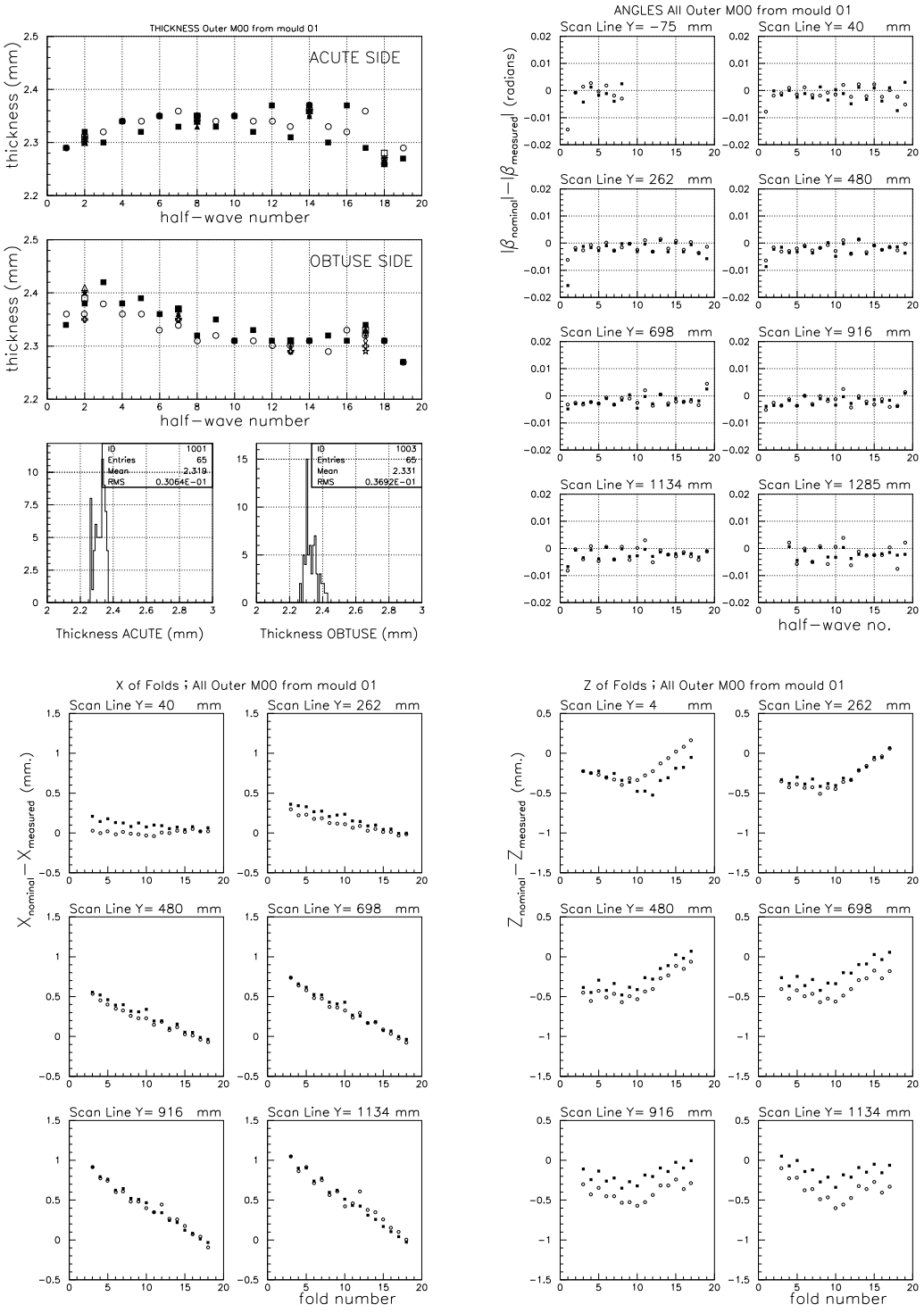


Figure 23: Thickness, angles and X and Z coordinate results from the measured absorbers cured in mould no. 1. The full square correspond always to b050_01_m00c01.

## 4.4 Other measurements done in the Quality Control

The width of the absorber (between longitudinal bars) at its most acute and obtuse extremes was measured both during the basic quality control (by means of a caliber) and during the extensive quality control (with the 3-D measuring machine). See secs. 2.1 and 2.2 for details. The summary of these width measurements is shown in Fig. 24. The following comments are worth:

1. Based on the gaussianity of the distributions we may conclude that the measurement with caliber is more reliable at the acute side (width1) than at the obtuse side (width2). This was expected due to the larger measurement surface of the longitudinal bars at the former position.

2. Also based on gaussianity, the measurement with the 3-D machine seems less reliable than expected. This may be an indication that some absorbers are not fully free in the transverse direction when placed on the measuring jig.

3. We do not see a clear dependence of the measured width neither on the autoclave cycle nor on the mould in which the absorber has been cured.

4. From these width measurements we establish an absorber shrinkage of 1 mm in the acute side and 0.3 mm in the obtuse side ( for the second estimate we take the results from the 3-D measurements). These estimates are reasonably similar to those obtained from the analysis of the X coordinates of the folds. They are also reasonably similar to what was predicted from the finite elements modelization for the curing process of the absorber [5] (1.6 and 0.3 mm respectively).

Also the absorber length was measured at two positions during the basic quality control. See sec. 2.2 for details. The summary of these length measurements is shown in Fig. 25. No particular comment is worth here.

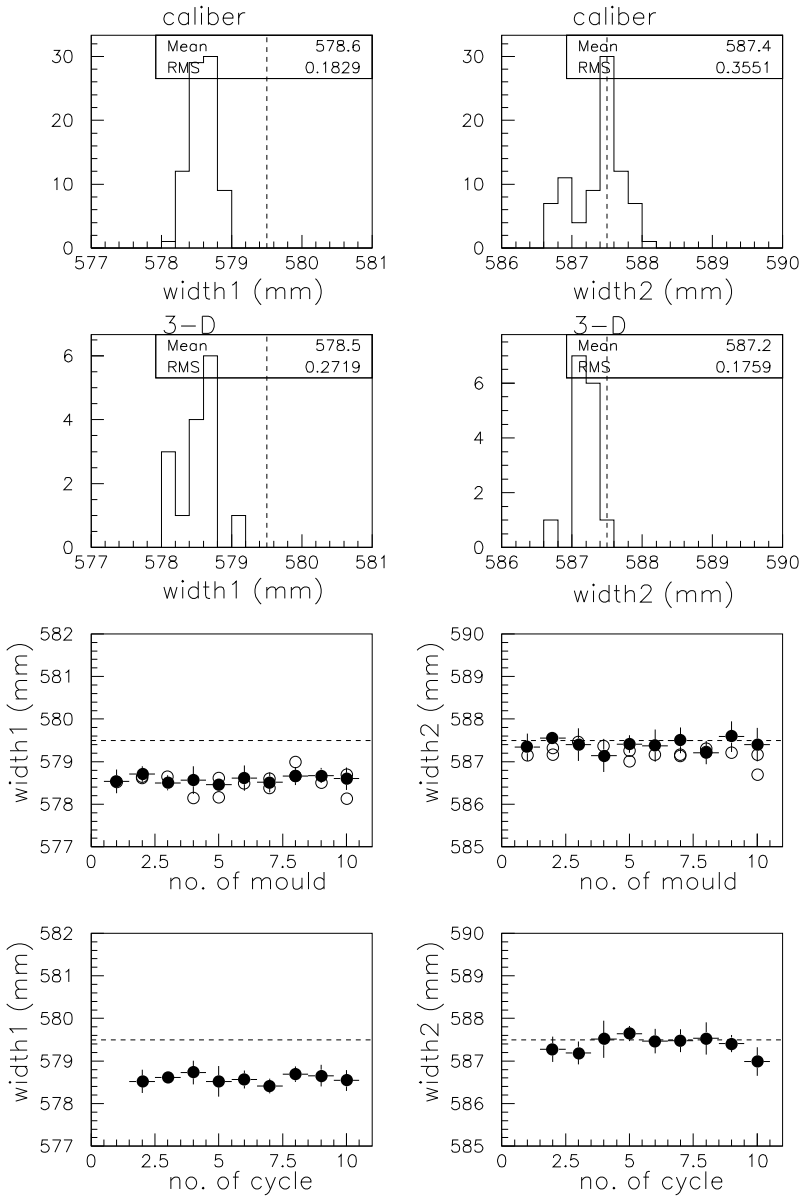


Figure 24: Measurements of outer absorber widths at their acute (width1) and obtuse (width2) sides. The histograms show the distributions obtained when using either the caliber or the 3-D machine for measuring. The first row of plots show the mean of the widths measured with the caliber as a function of the number of mould in which the absorber were cured (full circles). The error bars are the corresponding RMS. Overlaid are individual results from 3-D measurements (empty circles). The second (and last) row of plots show the mean (and RMS as errors) when grouped the caliber measurements by the production cycles. In all the cases the dashed lines are the nominal values.

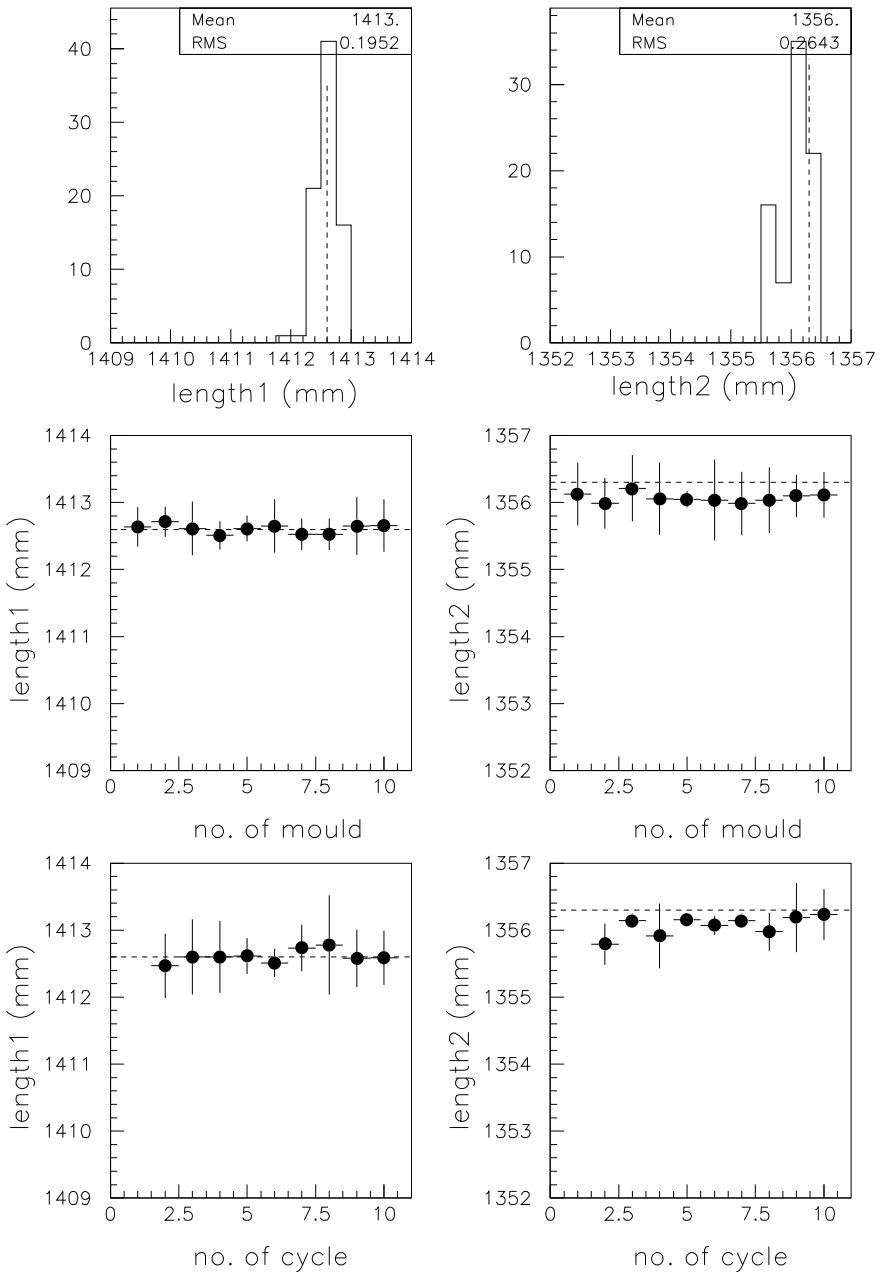


Figure 25: Measurements of outer absorber lengths. The histograms show the distributions obtained. The first row of plots show the mean of the measured length as a function of the number of mould in which the absorber was cured. The error bars are the corresponding RMS. The second (and last) row of plots show the mean (and RMS as errors) when grouped the measurements by the production cycles.

# 5 Analysis of measurements on inner absorbers.

## 5.1 Thicknesses.

Fig. 26 show all the thicknesses measured in all the M00 inner absorbers (except two of them, for which we will have a particular discussion) as a function of the half-wave number (see Fig. 3 for numbering convention) and in histograms. The measurements at the acute and obtuse sides of the absorbers are shown separately. Measurements from absorbers from the same mould have been given the same marker type. As in the outer absorber case, there is a clear systematic in the thickness along the absorber edges, being in this case of similar size in the acute and obtuse sides. Possible reasons for this systematics have been extensively discussed in section 4.1

Nevertheless, even with these systematics, the RMS of all the thickness measurements made at the acute and obtuse absorber sides is 43 $\mu m$ and 48 $\mu m$, below the tolerance values of 110 $\mu m$ and 60 $\mu m$ respectively (see the histograms in Fig. 26).

In order to separate the systematic from edge effects along the absorber sides, from the thickness reproducibility in a given point, we present in Fig. 27 the mean and RMS of all the measurements done in every half-wave surface as a function of its half-wave number. The thickness RMS obtained in all the half-wave surfaces are always below 40 $\mu m$ and in many cases (almost all in the acute side) below 20 $\mu m$.

As we did for the outer absorbers we present in Fig. 28 a reproducibility study (from cycle to cycle) for the thickness measured in absorbers made in the same mould (in this case mould no. 2). Good reproducibilities are obtained with RMS's typically below or around 15 $\mu m$. The same analysis in the rest of the moulds show similar features (not shown).

### 5.1.1 The case of absorbers s040_03_m00c01 and s032_04_m00c01

Fig. 29 shows the thickness measured in the inner absorbers made in the first cycle as a function of the half-wave number and also as histograms. The black squares and the up sided triangles correspond to the absorbers made in moulds no. 1 and 2 respectively. Down sided triangles and open circles are from absorbers made in moulds no. 3 and 4. It is apparent that the latter couple are systematically higher than the former.

The reason for the above effect was a longitudinal displacement (about 1.5 $mm$) of the top mould part w.r.t. to the bottom part (in the direction from obtuse to acute) in moulds no. 3 and 4 during the curing cycle.

Moulds no. 3 and 4 were the last moulds manufactured in the process of EMEC absorber tooling fabrication. They have a different design, similar to those for the outer absorbers, than moulds no. 1 and 2. The reason for this change in dessing was the significant lower price of the new approach which had previously been successfully tested in the commissioning phase of the moulds for the inner absorbers. The problem we didn't foresee was that due to the much smaller surface area of the inner absorber, the difference in force transmitted by the mould to the absorber surface between the acute and obtuse sides because of the different relative angle between the mould external surface and the wave surface, was larger than the friction between the absorber and mould surfaces and therefore able to induce that displacement (there is not measurable displacement in the outer absorber mould parts which have a 4 times larger surface area).

After adding a device in moulds no. 3 and 4 to prevent the above displacements, the thickness differences were largely reduced (see Fig. 26).

However, there are still some extra problems in moulds no. 3 and 4 which make the thicknesses measured in their absorbers to be still slightly above those from moulds no. 1 and 2 (look carefully to Fig. 26; the black squares and the up sided triangles correspond to the absorbers made in moulds no. 1 and 2 respectively, whereas down sided triangles and open circles are from absorbers made in moulds no. 3 and 4). The source of these effects remains unknown; our current hypothesis is that they come from the different transversal stifness of both mould types (larger for that of 1 and 2) which translates into a different mould deformation at the absorber edges (see sec. 4.1).

Nevertheless, in all the cases thickness RMS's are within tolerances (see Figs. 26, 27 and 29).

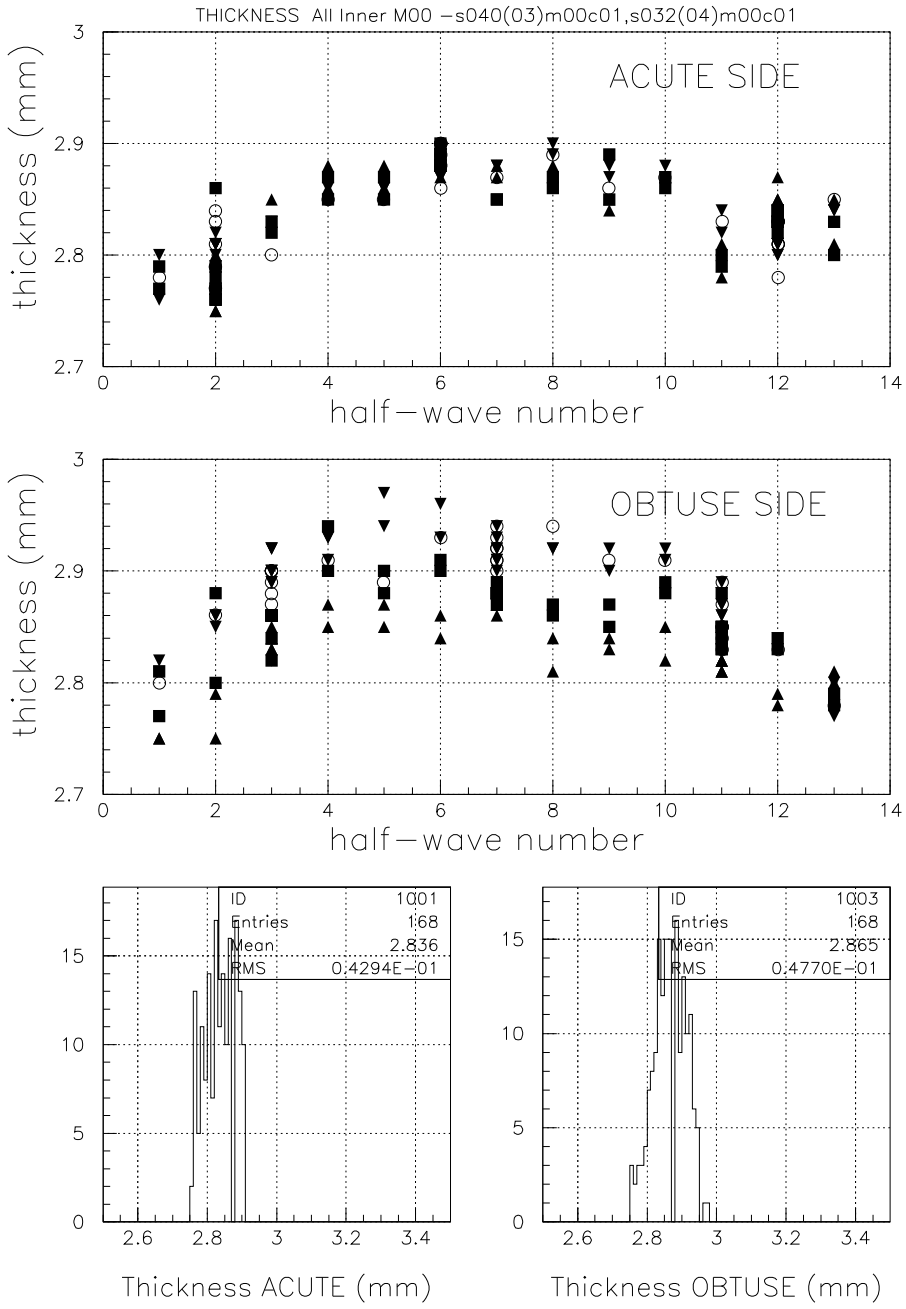


Figure 26: Thicknesses measured at the acute and obtuse sides of all the inner absorbers produced for M00 (except the two indicated in the figure's title) as a function of the number of the half-wave surface where the thickness was actually measured (top and middle plots). Measurements from absorbers from the same mould have been given the same marker type. Bottom plots: histograms for all these thicknesses measured. The tolerances for the thickness RMS are 0.110 *mm* and 0.060 *mm* in the acute and obtuse sides respectively.

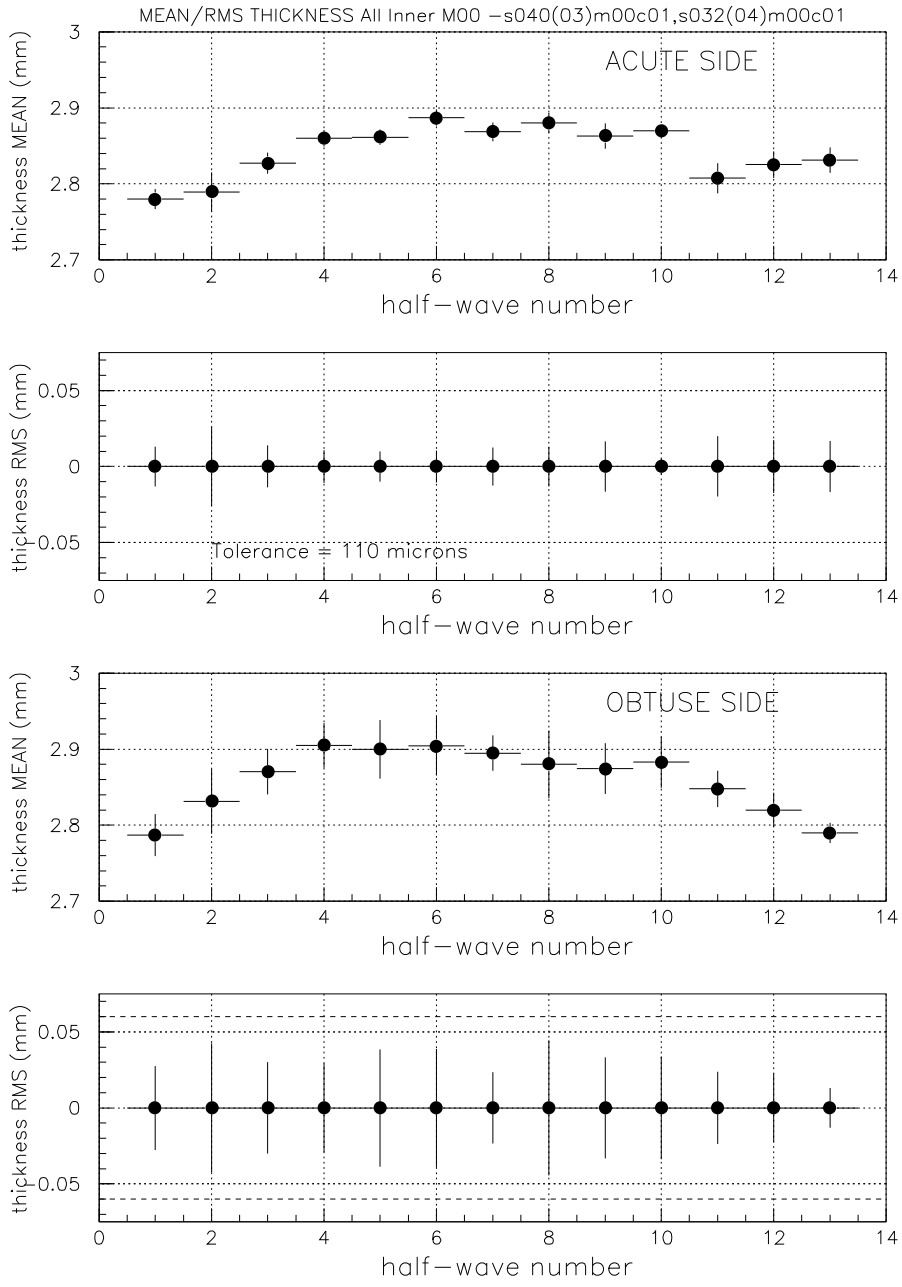


Figure 27: Mean and RMS of all the thicknesses measured in a given half-wave surface as a function of its number. The results from all the M00 inner absorbers produced, except the two indicated in the figure's title, have been included. In the RMS plots, the results are shown as error bars on points set at 0. These error bars are the same as those in the plots for the mean. The tolerances for the RMS in the obtuse side are indicated by two dashed lines.

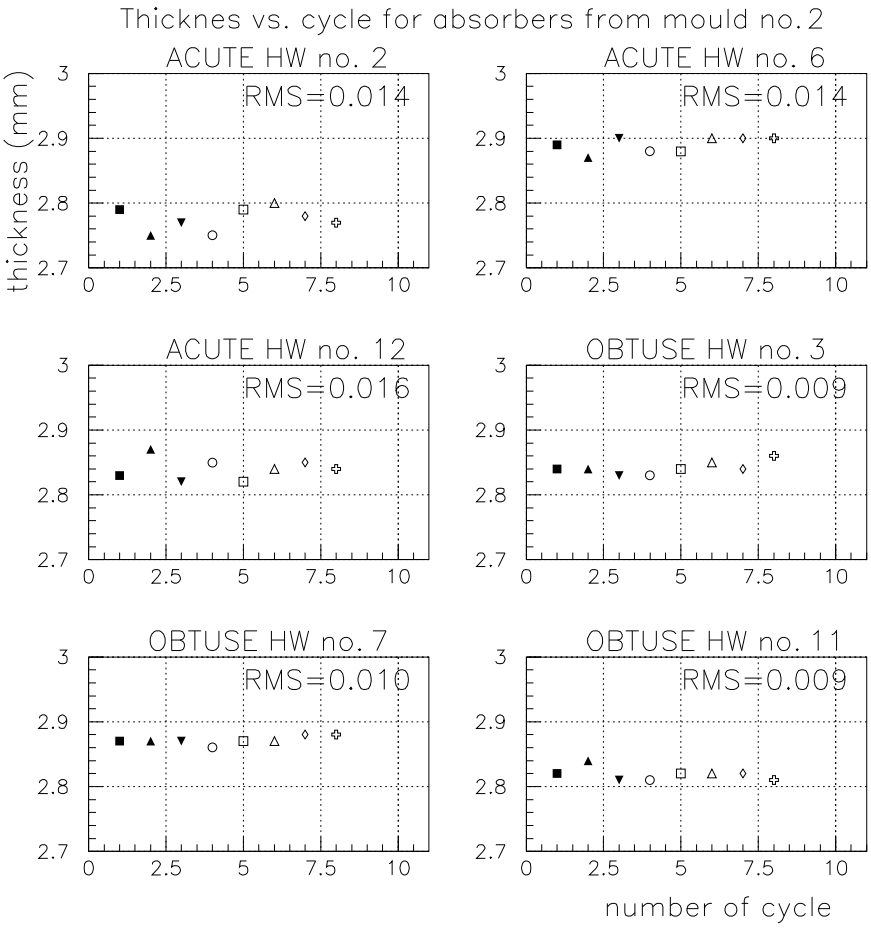


Figure 28: Inner absorbers made at mould no. 2: thicknesses measured in 3 fixed half-wave surfaces at both, acute and obtuse sides, as a function of the number of the cycle in which the particular absorber was produced.

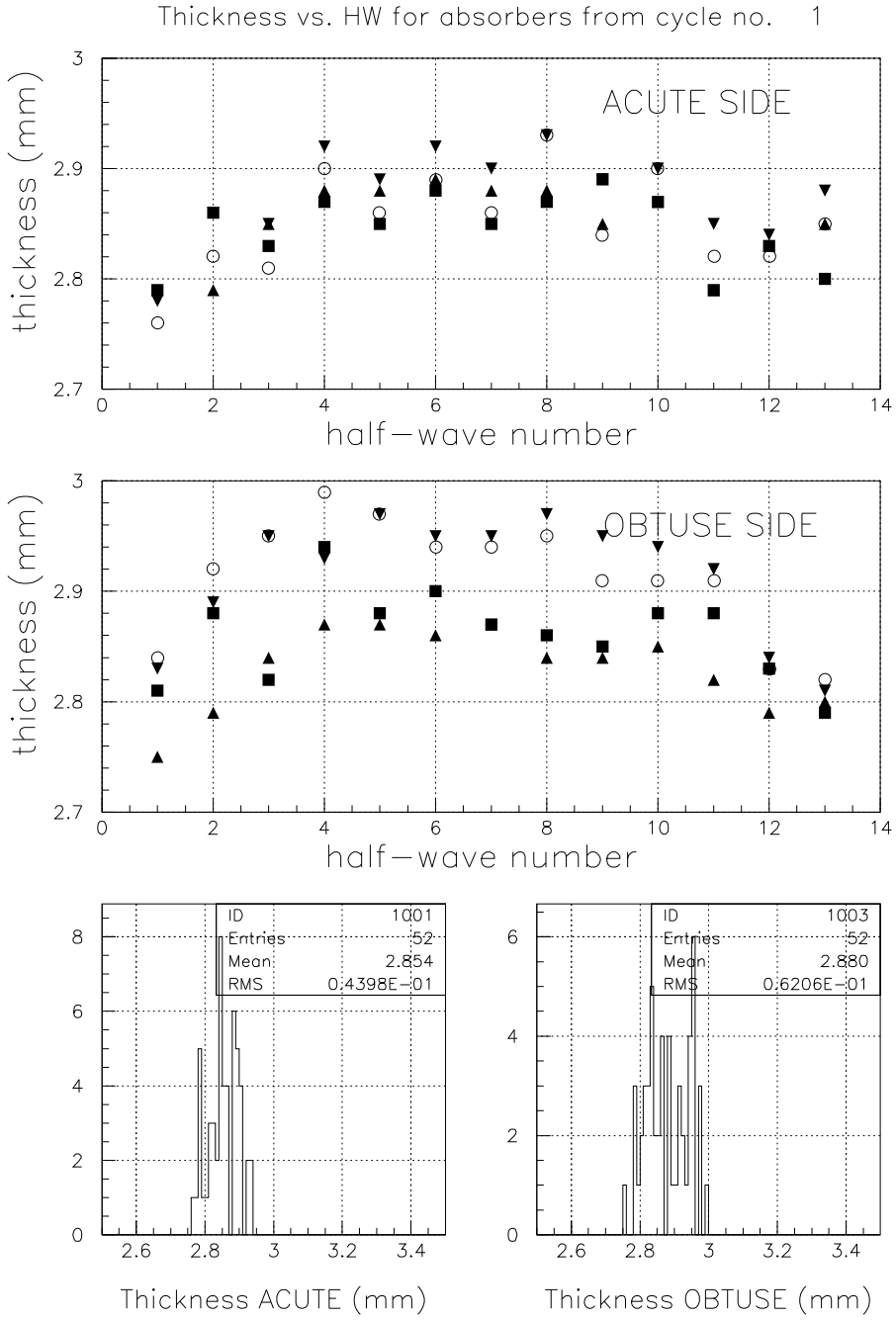


Figure 29: Inner absorbers made in the first cycle: thicknesses measured at the acute and obtuse sides as a function of the number of the half-wave surface where the thickness was actually measured (top and middle plots). Black squares and up sided triangles (down sided triangles and empty circles) correspond to the absorbers made in moulds 1 and 2 (3 and 4) respectively. Bottom plots: histograms for all these thicknesses measured. The tolerances for the thickness RMS are 0.110 *mm* and 0.060 *mm* in the acute and obtuse sides respectively.

## 5.2 Angles of the half-wave surfaces.

Fig. 30 show the deviations w.r.t. nominal of the measured half-wave surface's angle as a function of the half-wave surface no. and at the seven scan lines. Notice that the lowest Y value corresponds to the obtuse side of the absorber whereas the highest Y value is at its acute side. See Fig. 6 for reference frame. Data from all the 3D measured M00 inner absorbers are shown. Absorbers from the same mould are given the same marker type.

As in the outer absorber case, we have also included in Fig. 30 the measurements at half wave surfaces no. 1 and 13 despite of their much worse angular measurement resolution as discussed in sec. 3.2.

One can comment the following features of the data displayed in Fig. 30:

1. The measured $\beta$ angles are in general larger (in absolute value) than nominal, i.e. the produced absorbers have acuter folds, see Fig. 6, than designed. As in the outer absorber case, these acuter folds are believed to be a reflection from a global absorber transversal shrinkage.

2. In this case, the jitter in the measured angles only shows up in the internal and external absorber sides being the angles at the interior rather stable. On the other hand, the magnitude of the jitter at the internal side surface is large, increasing as we move towards the acute side. The source of this large jitter is not known. Our first guess was a problem in one of the knives of the press. We did carefully investigate their dimensions and location within the press and also their behavior during the folding process without observing any clear defect. Our current hypothesis is that it comes from a non uniform shrinkage of the absorber due to its particular geometry (its external side is substantially longer than its internal side). This and the previous systematic effects are better seen in Fig. 33 (see below for the explanation of its contents).

3. All the absorbers show similar behavior. If one looks carefully to Fig. 30 though, one can appreciate the results from absorbers s040_03_m00c01 and s032_04_m00c01 (full down-triangles and open circles respectively) slightly above the bulk at the obtuse side.

Fig. 31 show the distributions for the deviations w.r.t. nominal of all the measured half-wave surface's angles at the seven scan lines. The measurements at half-wave nos. 1 and 13 have not been included. The RMS tolerances are given in radians; they vary longitudinally as the LArg. gap does. The measured R.M.S.'s are above the tolerances established in sec. 2.3 by a factor of around 5/4 being the large jitter of the first fold the responsible of the large dispersion. If we did not include those folds, the measured R.M.S. would be within tolerances (see Fig. 32). The mean deviation w.r.t. nominal of the measured angles is around 2.5 milliradians.

In order to separate systematic effects from the reproducibility in a given point, we present in Fig. 33 the mean and RMS of all the measurements (always w.r.t. nominal) from every half-wave surface as a function of its half-wave number and at six scan lines. The evolution of the angle jitter discussed above appears very clear in Fig. 33. The angle RMS obtained point-to-point are in most cases well below tolerances. The typical reproducibility is 1.5 milliradians RMS.

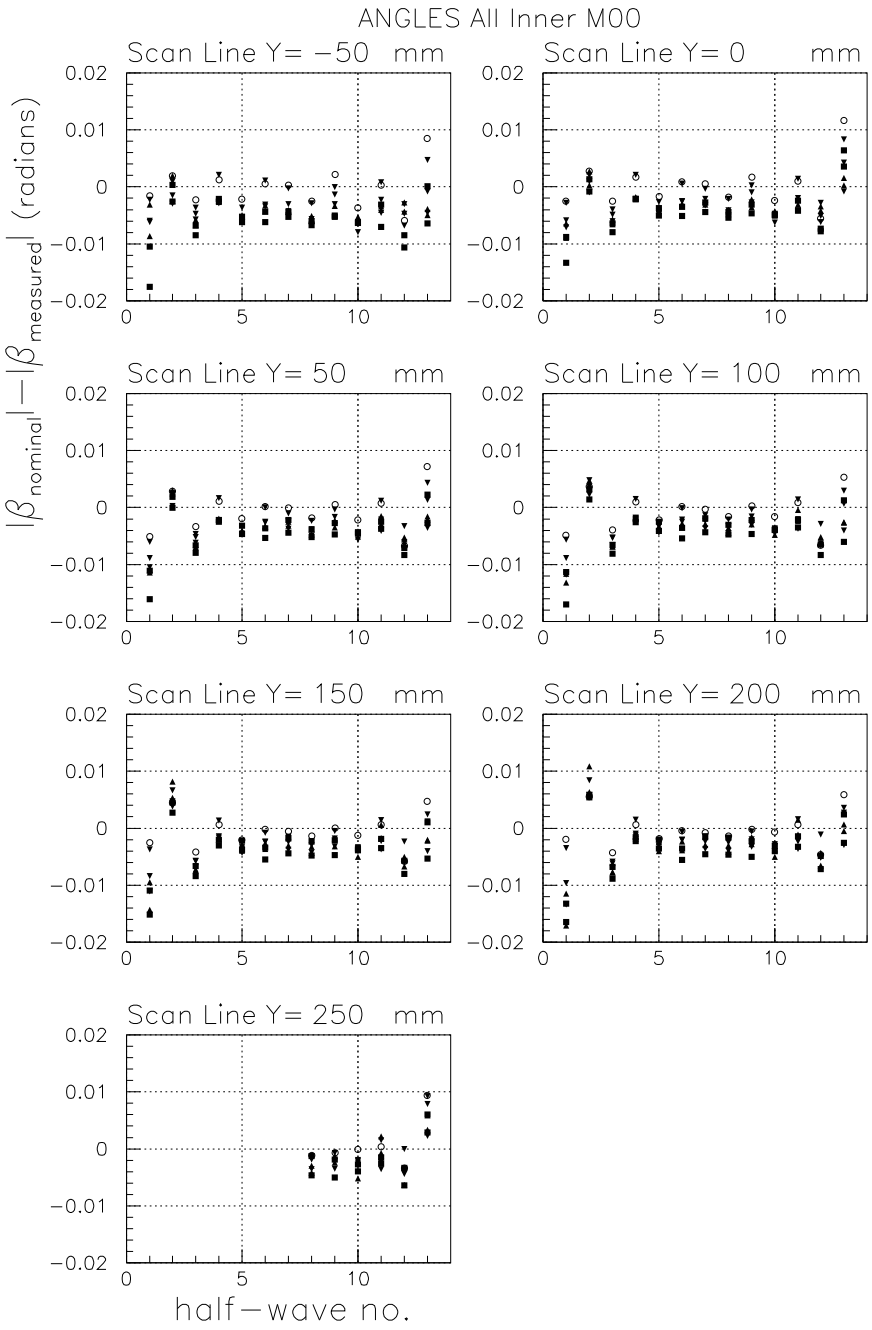


Figure 30: Deviations w.r.t. nominal of the measured half-wave surface angle as a function of the half-wave no. and at the seven scan lines. Data from all the 3D measured M00 inner absorbers are shown. Absorbers from the same mould are given the same marker type. The lowest Y value is at the obtuse side of the absorber; the highest Y value is at its acute side.

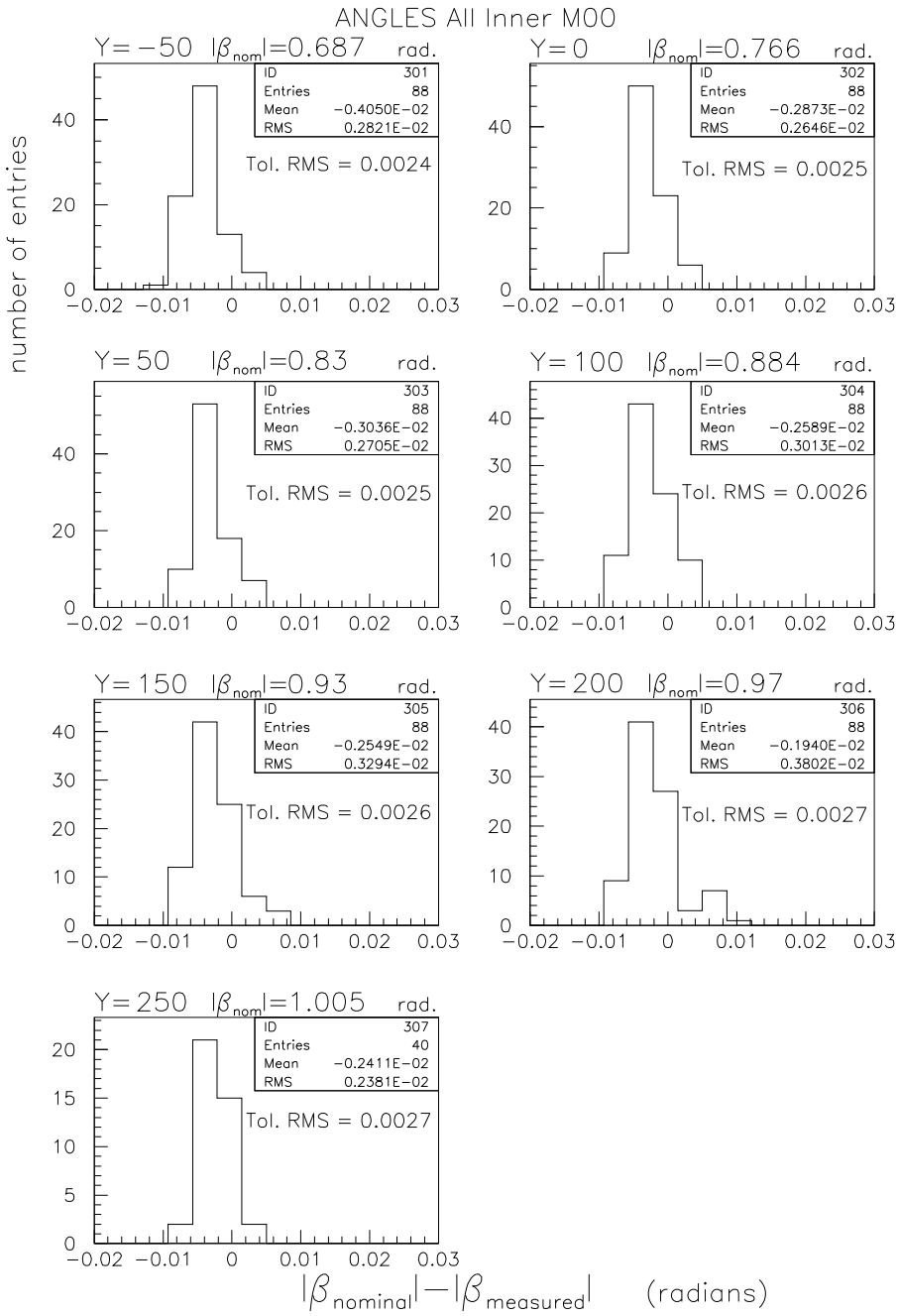


Figure 31: Histograms for the deviations w.r.t. nominal of the measured half-wave surface's angle at the seven scan lines. Data from all the 3D measured M00 inner absorbers are shown. The RMS tolerances are given in radians. The lowest Y value is at the obtuse side of the absorber; the highest Y value is at its acute side.

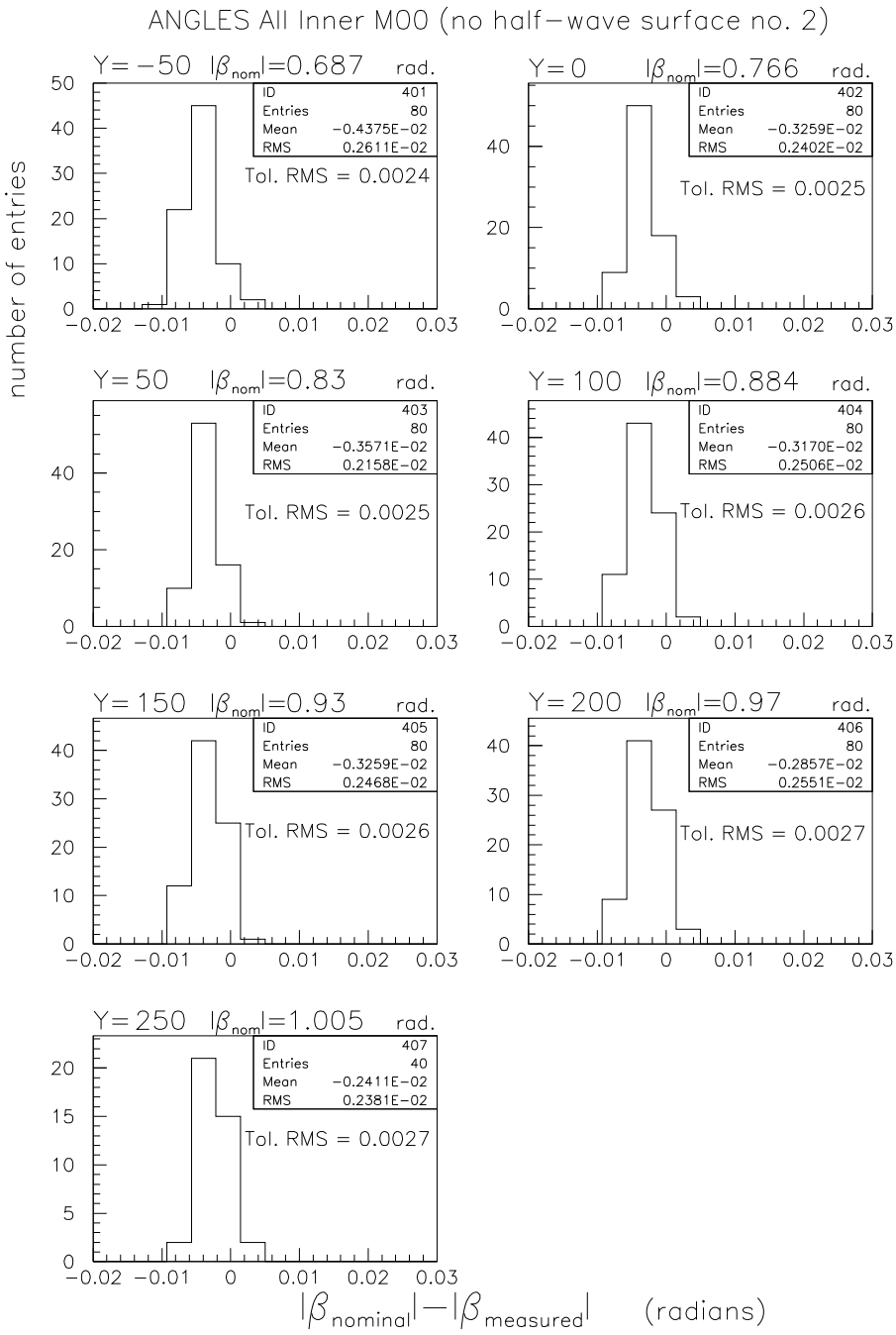


Figure 32: Histograms for the deviations w.r.t. nominal of the measured half-wave surface's angle at the seven scan lines. Data from all the 3D measured M00 inner absorbers (except the measurements at half-wave no. 2) are shown. The RMS tolerances are given in radians. The lowest Y value is at the obtuse side of the absorber; the highest Y value is at its acute side.

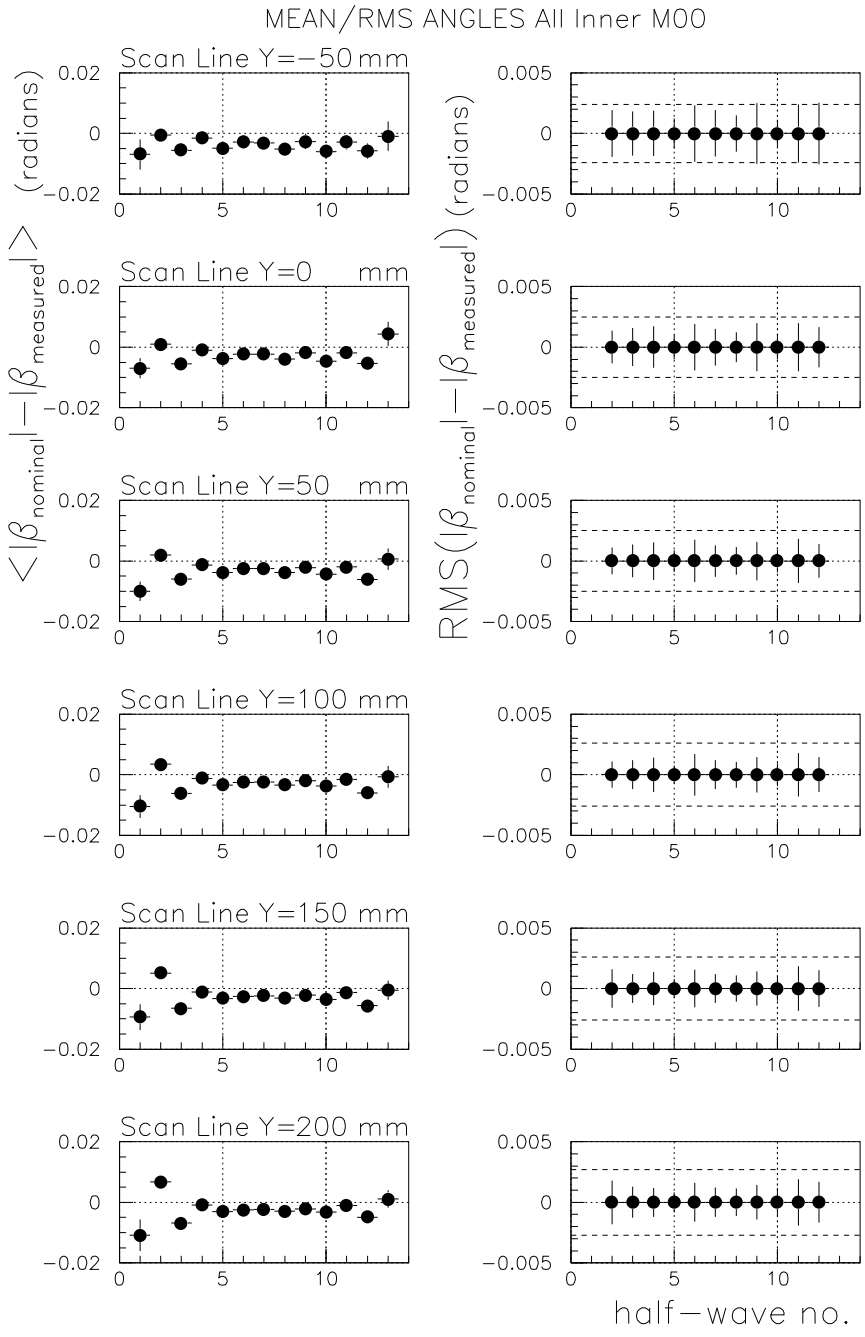


Figure 33: Mean and R.M.S. of the deviations w.r.t. nominal of the measured half-wave surface's angle in a given half-wave as a function of its number and at six scan lines. Data from all the 3D measured M00 inner absorbers are shown. The R.M.S. results are shown as error bars on points at 0. These error bars are the same as those in the plots for the mean. The tolerances for the RMS are indicated by the dashed lines. The lowest Y value is close to the obtuse side of the absorber; the highest Y value is close to its acute side.

## 5.3 Fold's coordinates.

In this subsection we study the reconstructed X and Z coordinates of the absorber fold's along the six lines where a full transverse scan was carried out. See Fig. 6 for details of the reconstruction method.

Fig. 34 show the deviations w.r.t. nominal of the measured X coordinate of the folds as a function of the fold no. for the six scan lines. Data from all the 3D measured M00 inner absorbers are shown. It is apparent the absorber shrinkage that we envisaged when analyzing the angles. The magnitude of the shrinkage increases almost linearly with Y. There is no absorber deviating clearly from the rest.

In order to separate systematic effects from the reproducibility in a given point, we present in Fig. 35 the mean and R.M.S. of all the X measurements (always w.r.t. nominal) from every fold as a function of its fold number and at the six scan lines. From the plots for the means we estimate a shrinkage of approximately 1.3 (0.9) mm at the acute (obtuse) side. The R.M.S. of the measurements from all absorbers in a given fold position are typically 50 (100) $\mu m$ in the obtuse (acute) sides, within tolerances in all the cases.

Fig. 36 show the deviations w.r.t. nominal of the measured Z coordinate of the folds as a function of the fold no. for the six scan lines. Data from all the 3D measured M00 inner absorbers are shown. In contrast to the outer absorber case, no apparent absorber twist is observed (see also Fig. 37), but only a slight deformation upwards (recall the reference frame from sec. 3.2). There is also no large dispersion in the obtuse-internal side, consistent with the better performance of the inner absorber measuring jig. Two absorbers deviate slightly from the rest at the acute side: s031_01_m00c01 and sun02_01_m00c01. We have no explanation for that deviation.

Fig. 37 shows the mean and R.M.S. of all the Z measurements (always w.r.t. nominal) from every fold as a function of its fold number and at the six scan lines. The effects discussed above are clearly seen either in the plots for the means or those for the RMS. The local dispersions vary from around 75 $\mu m$ RMS at the obtuse side to 200 $\mu m$ RMS at the acute side and are reasonable well within tolerances (notice that all the absorbers have been included). As in the outer absorber case the point to point jitter from the Z coordinate reconstructed method, is apparent in the plots for the mean.

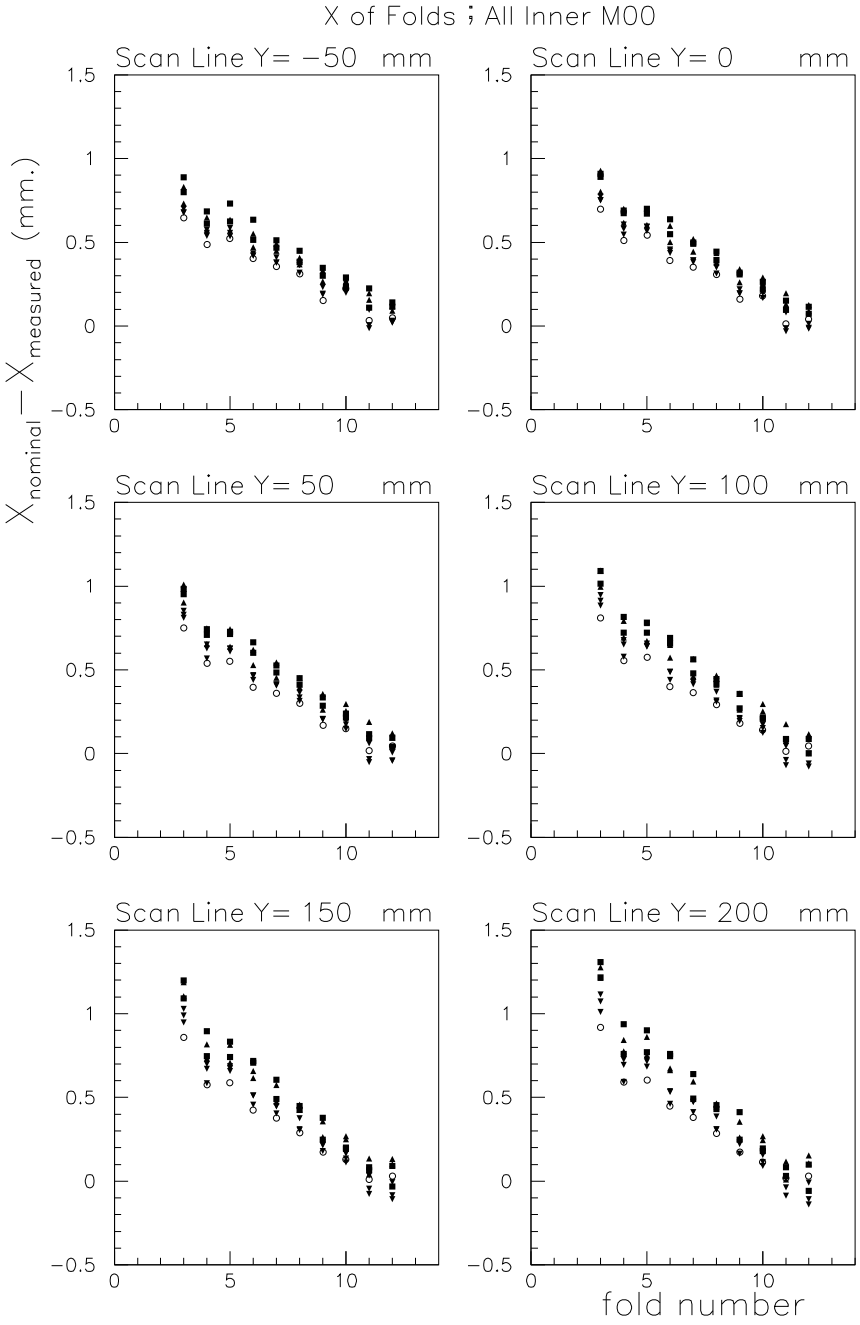


Figure 34: Deviations w.r.t. nominal of the measured X coordinate of the folds as a function of the fold no. and at six scan lines. Data from all the 3D measured M00 inner absorbers are shown. Absorbers from the same mould are given the same marker type. The lowest Y value is close to the obtuse side of the absorber; the highest Y value is close to its acute side.

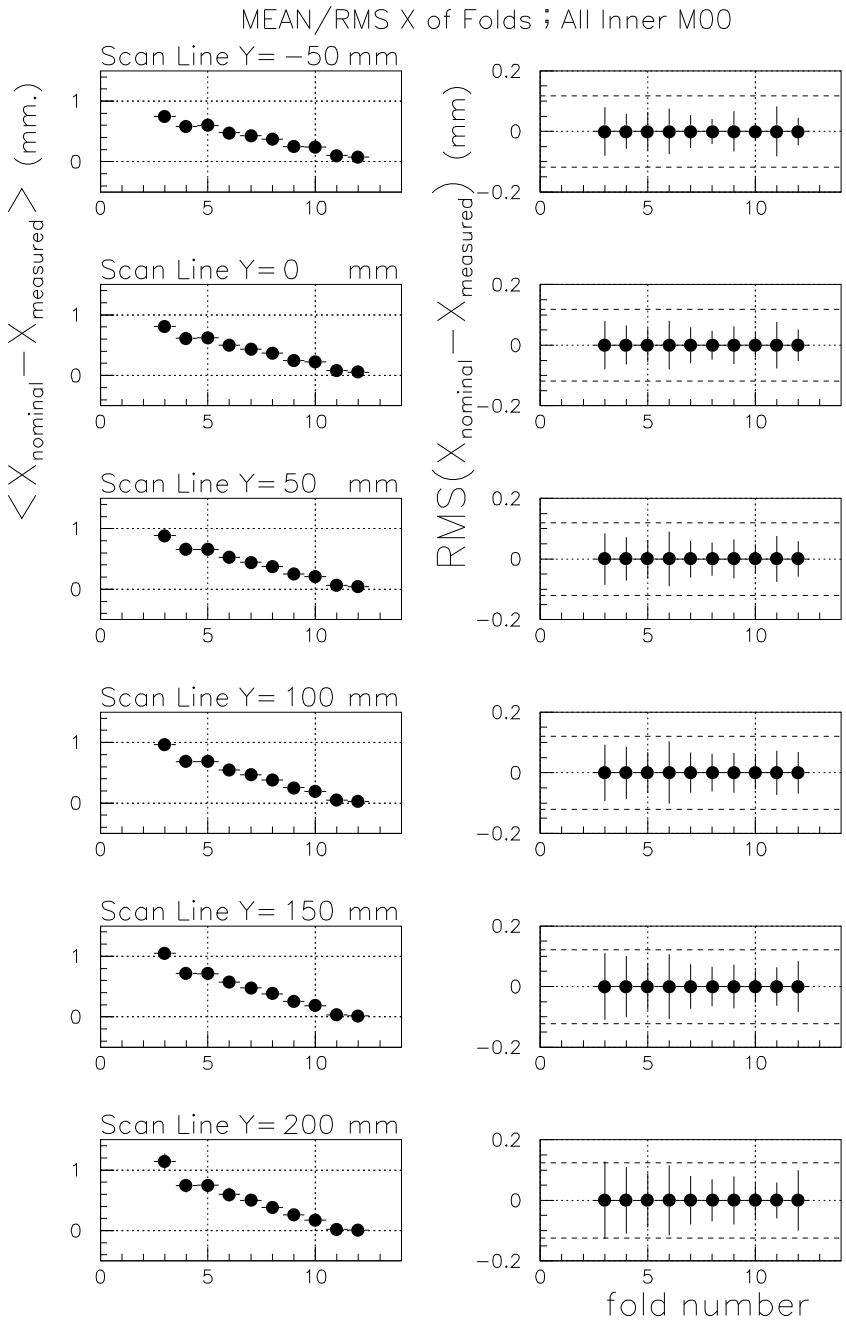


Figure 35: Mean and R.M.S. of the deviations w.r.t. nominal of the measured X coordinate in a given fold position as a function of its number and at six scan lines. Data from all the 3D measured M00 inner absorbers are shown. The R.M.S. results are shown as error bars on points at 0. These error bars are the same as those in the plots for the mean. The tolerances for the RMS are indicated by the dashed lines. The lowest Y value is close to the obtuse side of the absorber; the highest Y value is close to its acute side.

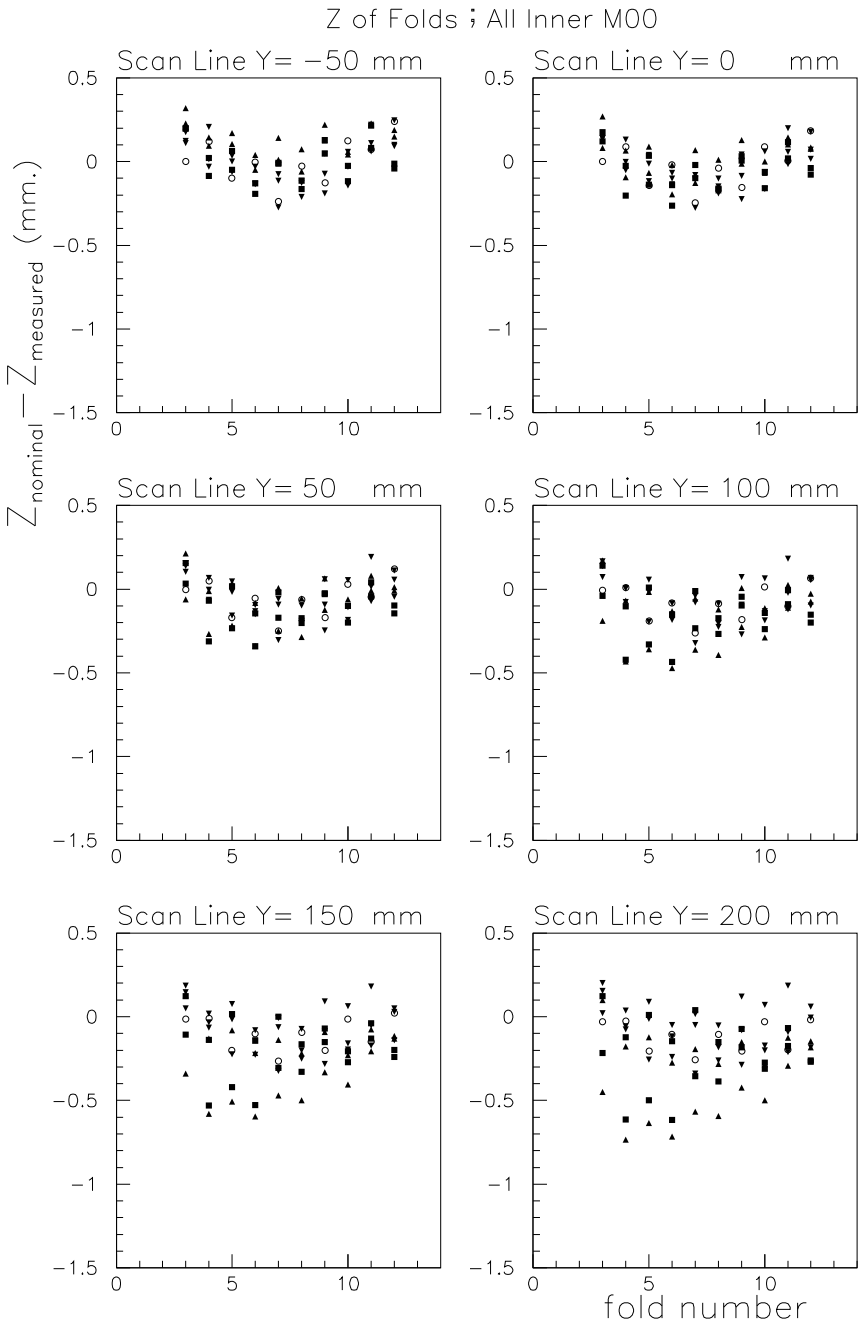


Figure 36: Deviations w.r.t. nominal of the measured Z coordinate at the folds as a function of the fold no. and at six scan lines. Data from all the 3D measured M00 inner absorbers are shown. Absorbers from the same mould are given the same marker type. The lowest Y value is close to the obtuse side of the absorber; the highest Y value is close to its acute side.

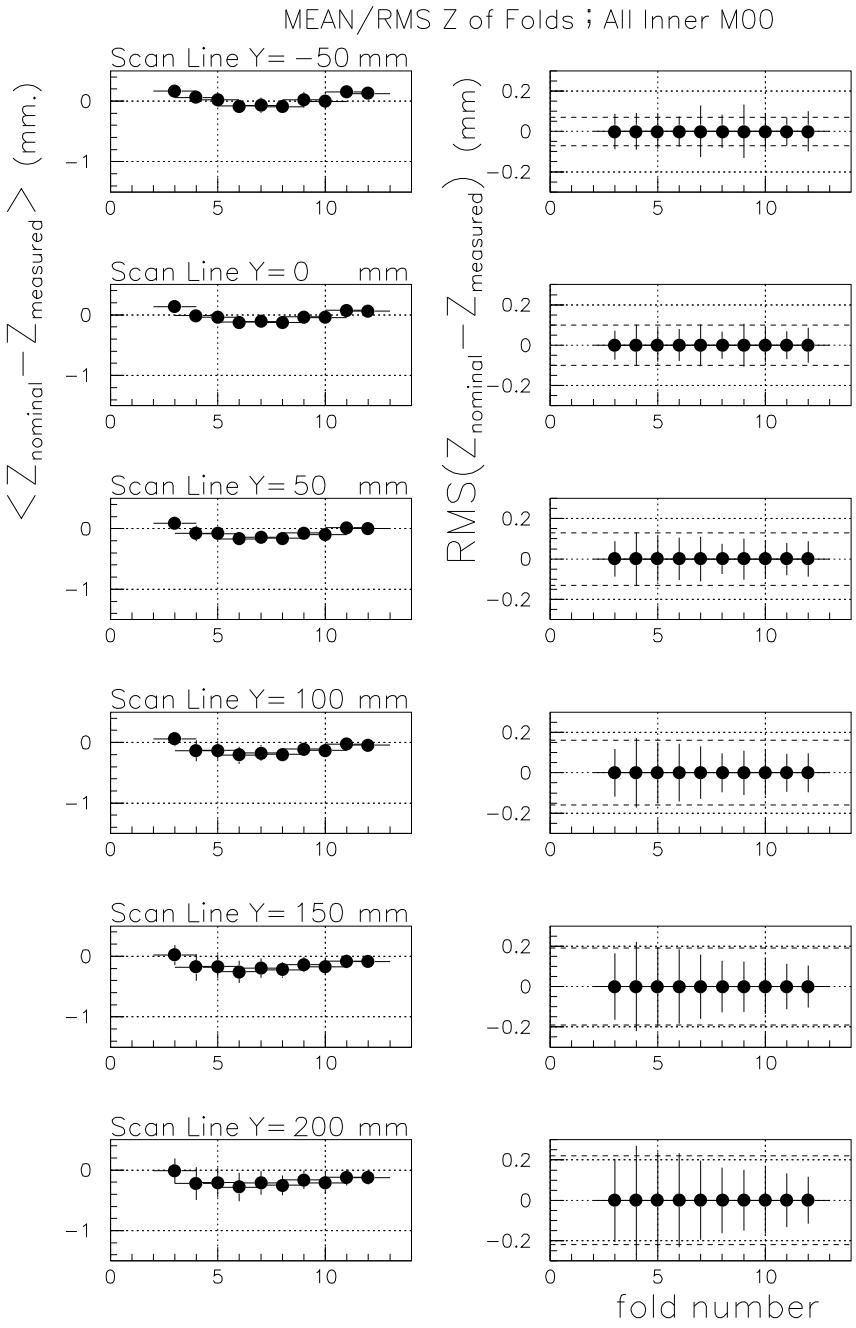


Figure 37: Mean and R.M.S. of the deviations w.r.t. nominal of the measured Z coordinate in a given fold position as a function of its number and at six scan lines. Data from all the 3D measured M00 inner absorbers are shown. The R.M.S. results are shown as error bars on points at 0. These error bars are the same as those in the plots for the mean. The tolerances for the RMS are indicated by the dashed lines. The lowest Y value is close to the obtuse side of the absorber; the highest Y value is close to its acute side.

## 5.4 Other measurements done in the Quality Control

We discuss now the measurements of absorber width (between longitudinal bars) at its most acute and obtuse extremes which were performed both during the basic quality control (by means of a caliber) and during the extensive quality control (with the 3-D measuring machine). See secs. 2.1 and 2.2 for details. The summary of these width measurements is shown in Fig. 38. Similar conclusions than for the outer absorber case are arrived to.

From these width measurements we estimate an absorber shrinkage of 1.3 mm in the acute side and 0.7 mm in the obtuse side ( for both estimates we take the results from the caliber measurements). These estimates are reasonable similar to those obtained from the analysis of the X coordinates of the folds. They are also reasonably similar to what was predicted from the finite elements modelization for the curing process of the absorber [5] (1.6 and 0.6 mm respectively). Notice that the inner absorbers shrunk slightly more than the outer absorbers, in particular at the obtuse side.

Also the absorber length was measured at two positions during the basic quality control. See sec. 2.2 for details. The summary of these length measurements is shown in Fig. 39. As in the case of the outer absorbers, no particular comment is worth here.

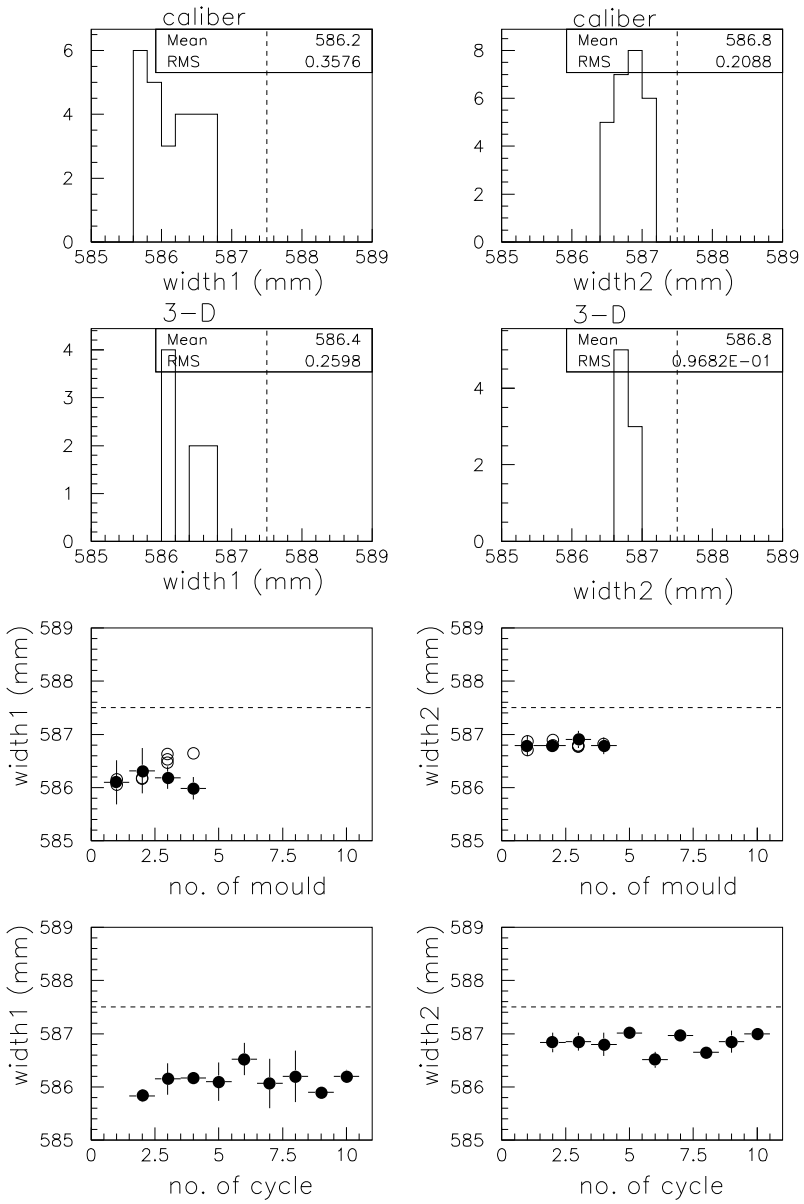


Figure 38: Measurements of inner absorber widths at their acute (width1) and obtuse (width2) sides. The histograms show the distributions obtained when using either the caliber or the 3-D machine for measuring. The first row of plots shows the mean of the widths measured with the caliber as a function of the number of mould in which the absorber were cured (full circles). The error bars are the corresponding RMS. Overlaied are individual results from 3-D measurements (empty circles). The second (and last) row of plots shows the mean (and RMS as errors) when grouped the caliber measurements by the production cycles. In all the cases the dashed lines are the nominal values.

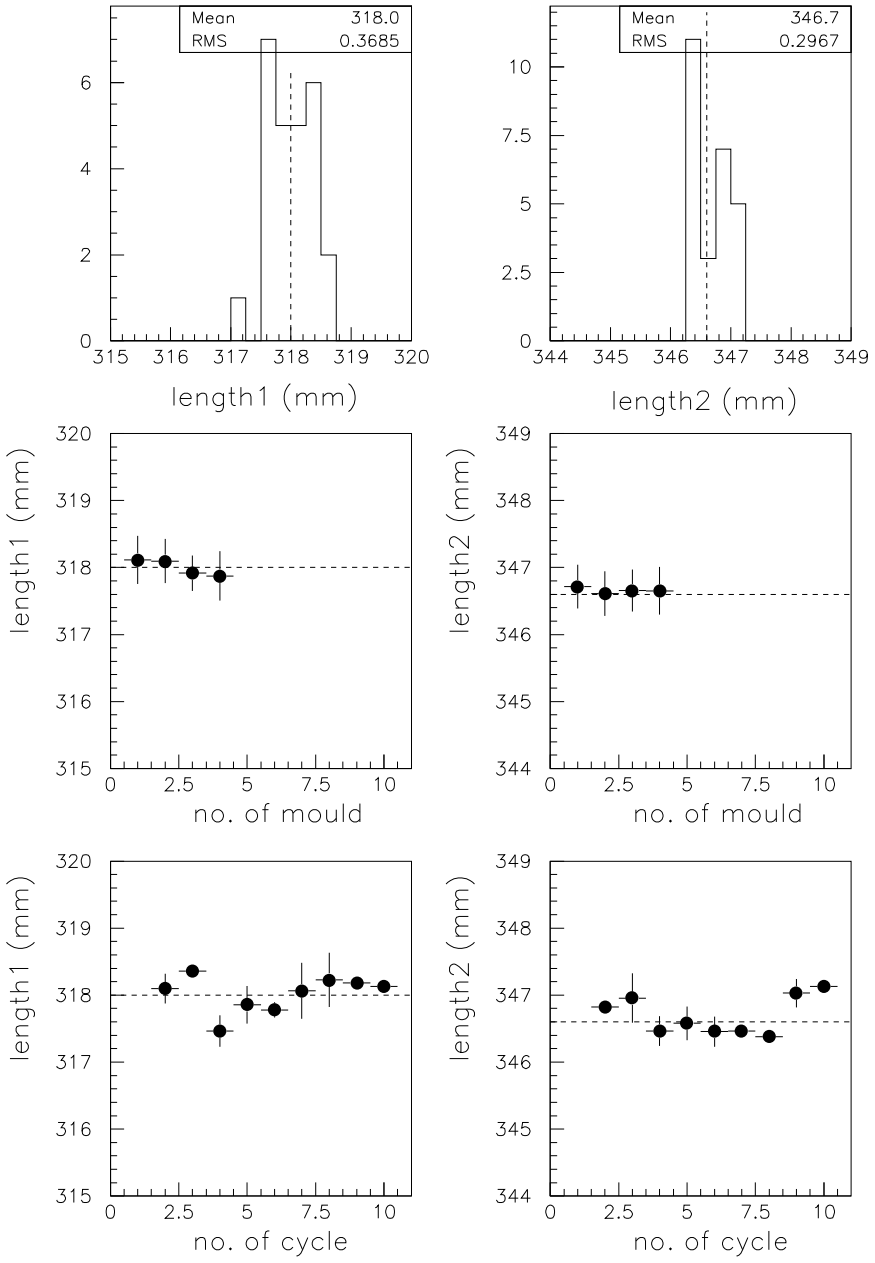


Figure 39: Measurements of inner absorber lengths. The histograms show the distributions obtained. The first row of plots show the mean of the measured length as a function of the number of mould in which the absorber were cured. The error bars are the corresponding RMS. The second (and last) row of plots show the mean (and RMS as errors) when grouped the measurements by the production cycles.

# 6 Summary

The measurements performed during the quality control procedure of the absorber production for the module 0 of the ATLAS electromagnetic EndCap calorimeter have been fully analyzed in this note.

Overall, the geometrical properties of the produced absorbers guarantee the 3 % Liquid Argon gap uniformity necessary to keep the constant term in the energy resolution at the target value.

The outer absorbers show thicknesses RMS of 26 $\mu m$ and 34 $\mu m$ at the acute and obtuse sides respectively. The reproducibility of the measured angles of the half-wave surfaces is at the 2.4 milliradians level. The X (transverse) and Z (height) coordinates of the folds show absorber to absorber dispersions of 75 $\mu m$ in average. The produced absorbers present a shrinkage which translates into a width reduction from 0.3 mm up to 1 mm from the obtuse to the acute sides.

The inner absorbers show thicknesses RMS of 43 $\mu m$ and 48 $\mu m$ at the acute and obtuse sides respectively. The reproducibility of the measured angles of the half-wave surfaces is at the 2.9 milliradians level. The X (transverse) coordinate of the folds show absorber to absorber dispersions of 75 $\mu m$ in mean. The corresponding dispersion of the Z (height) coordinate is around 150 $\mu m$. The measured shrinkage is from 0.8 mm up to 1.3 mm from the obtuse to the acute sides.

Some absorbers showed worse geometrical properties than the bulk. They were traced back to failures in the production process which have been fixed.

For the outer absorbers the worse results are obtained at their obtuse side. We suspect that the reason for them is not on the absorbers themselves (maybe partially on the longitudinal bars) but in the jig used for the 3-D measurements which does not guaranty their reproducibility. We will try to optimize this jig for the full production. There are, of course, some other minor effects which are not yet understood.

# References


[1] C. V. Scheel; ATLAS internal Note CAL-NO-079 (January 1996).

[2] P. Romero, L. Labarga; Geometrical tolerances for the absorbers, physics considerations; ABS.YYY.00.DRb.1; March 1998.

[3] P. Romero; The drawings for the outer absorber measuring jig are the ABS.QAP.20.(GDa.1, DDa.1 ... DDq.1). For the inner absorber jig are the ABS.QAP.10.(GDa.1, DDa.1 ... DDf.1). For general

[4] L. Labarga; Analysis of the 3-D measurements preformed on the last 8 outer absorber moulds manufactured by Talleres ARATZ; document prepared for internal discussions with Talleres ARATZ; February 1998.

[5] P. Romero; Liquid Argon Electromagnetic Calorimeter for ATLAS. EndCap Absorbers with Constant Lead Thickness: Thermal Expansion Coefficient. ATL-LARG-97-075, May 1997.